Ultraviolet and Visible Photochemistry of Methanol at 3D Mesoporous Networks: TiO2 and Au−TiO2

ARTICLE *in* THE JOURNAL OF PHYSICAL CHEMISTRY C · JULY 2013

Impact Factor: 4.77 · DOI: 10.1021/jp312583w

7 AUTHORS, INCLUDING:

Dimitar Panayotov
Virginia Polytechnic Institute and State Univer…
28 PUBLICATIONS **1,287** CITATIONS
SEE PROFILE

Paul Desario
United States Naval Research Laboratory
8 PUBLICATIONS **105** CITATIONS
SEE PROFILE

Lindsey Szymczak
Northwestern University
2 PUBLICATIONS **10** CITATIONS
SEE PROFILE

THE JOURNAL OF PHYSICAL CHEMISTRY C

Article

pubs.acs.org/JPCC

Ultraviolet and Visible Photochemistry of Methanol at 3D Mesoporous Networks: TiO_2 and Au−TiO_2

Dimitar A. Panayotov

Institute of General and Inorganic Chemistry, Bulgarian Academy of Sciences, Sofia 1113, Bulgaria

Paul A. DeSario,[§] Jeremy J. Pietron,*[,§] Todd H. Brintlinger,[‡] Lindsey C. Szymczak,[§] and Debra R. Rolison[§]

[§]Surface Chemistry Branch (Code 6170) and [‡]Materials & Sensors Branch (Code 6360), U.S. Naval Research Laboratory, Washington, D.C. 20375, United States

John R. Morris*

Department of Chemistry, Virginia Tech, Blacksburg, Virginia 24061-0212, United States

Supporting Information

ABSTRACT: Comparison of methanol photochemistry at three-dimensionally (3D) networked aerogels of TiO_2 or Au−TiO_2 reveals that incorporated Au nanoparticles strongly sensitize the oxide nanoarchitecture to visible light. Methanol dissociatively adsorbs at the surfaces of TiO_2 and Au−TiO_2 aerogels under dark, high-vacuum conditions. Upon irradiation of either ultraporous material with broadband UV light under anaerobic conditions, adsorbed methoxy groups act as hole-traps and extend conduction-band and shallow-trapped electron lifetimes. A higher excited-state electron density arises for UV-irradiated TiO_2 aerogel relative to commercial nanoparticulate TiO_2, indicating that 3D networked TiO_2 more efficiently separates electron−hole pairs. Upon excitation with narrow-band visible light centered at 550 nm, long-lived excited-state electrons are evident on CH_3OH-exposed Au−TiO_2 aerogels—but not on identically dosed TiO_2 aerogels—verifying that incorporated Au nanoparticles sensitize the networked oxide to visible light. Under aerobic conditions (20 Torr O_2) and broadband UV illumination, surface-sited formates accumulate as adsorbed methoxy groups oxidize, at similar rates, on Au−TiO_2 and TiO_2 aerogels. Moving to excitation wavelengths longer than ~400 nm (i.e., the low-energy range of UV light) dramatically decreases methoxy photoconversion for methanol-saturated TiO_2 aerogel, while Au−TiO_2 aerogel remains highly active for methanol photooxidation. The wavelength dependence of formate production on Au−TiO_2 tracks the absorbance spectrum for this material, which peaks at λ = 550 nm due to resonance with the surface plasmon in the Au particles. The photooxidation rate for Au−TiO_2 aerogel at 550 nm is comparable to that for TiO_2 aerogel under broadband UV illumination, indicating efficient energy transfer from Au to TiO_2 in the 3D mesoporous nanoarchitecture.

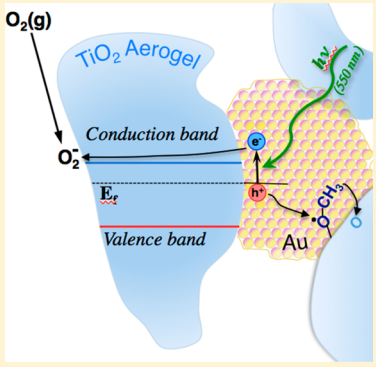

1. INTRODUCTION

High-surface-area nanostructured TiO_2 materials have tremendous potential to impact photocatalytic applications ranging from environmental remediation[1−4] to organic synthesis.[4] Titania photocatalysts are wide band-gap semiconductors that require ultraviolet (UV) photons with energies exceeding 3 eV to create the electron−hole pairs that drive catalytic oxidation−reduction chemistry. Because high-energy photon sources have many practical limitations and only 3−5% of the sunlight that reaches the earth falls into this region of the electromagnetic spectrum,[5] great effort has been expended in recent years on the development of new TiO_2-based materials that absorb visible light. One strategy dopes TiO_2 with metal or nonmetal ions to narrow the band gap or to create states within the band gap that effectively lower the overall excitation energy.[1,6−9] More recently, TiO_2-supported metallic nanostructures were shown to absorb visible radiation and generate electron−hole pairs.[6,7,10−20] Efficient absorption in these oxide-supported metal nanoparticles is due to resonance of the incident photons with collective oscillations of confined metallic valence electrons, known as plasmons.[6,7,12,16,18,20−23]

One of the most widely studied classes of nanostructured plasmonic metal/semiconductor systems for photocatalytic applications comprises TiO_2-supported Au (Au/TiO_2) or Pt

Received: December 20, 2012
Revised: May 23, 2013
Published: May 23, 2013

nanoparticles.[11,13,15−19,23−25] The wavelength dependence of the quantum efficiency for a given photocatalytic reaction at these materials, the so-called action spectrum, typically reaches a maximum precisely at the excitation energy of the local surface plasmon resonance (LSPR) of the material.[5,15,17,19,25] The exact energy profile of the surface plasmon band of metallic nanoparticles depends on factors such as the dielectric constant of the substrate, the size and shape of the particles, and their charge,[6,16,20,22,23] all of which subsequently affect the photocatalytic efficiency. Recent examples include correlating the efficiency of photooxidation of 2-propanol with size and shape of the metal particles as well as the surface area and crystallinity of the oxide support[15,17] and finding a strong dependence on Au particle size for the Au/rutile system with maximum photoactivity for 5-nm Au and only a weak size dependence for the Au/anatase system.[19] Linic et al. suggested that by manipulating the shape and size of the metal and semiconductor components in plasmonic nanostructures, it may be possible to design plasmonic systems that interact with the entire solar spectrum.[16] Detailed discussion of the mechanisms for SPR-mediated photocatalytic reactions and critical design parameters for plasmonic metal−semiconductor composite photocatalysts can be found in recent reviews.[6,16,20,22,23]

Mesoporous TiO_2 is an excellent host matrix for embedding plasmonic gold nanoparticles to produce Au/TiO_2 composites with enhanced photocatalytic activity.[25−32] Aerogels are a unique class of ultraporous materials that feature a scalable nanoscale solid network interpenetrated in three dimensions (3D) by a continuous network of meso- to small macropores, thereby creating an architecture with walls of high surface area (~100−1000 $m^2\ g^{-1}$) and 3D nanoscale plumbing that ensures facile transport of molecules.[33−35] Rolison and co-workers introduced the general modification strategy of guest−host composite aerogels in which the nanoscopic guest, added just as the host sol undergoes gelation, is not totally encapsulated by the nanoparticles comprising the aerogel network and thus is available to interact with molecular reactants traversing the pore network.[36,37]

Pietron et al. applied this strategy, in which metal nanoparticles are directly incorporated into the nanoparticle network of the aerogel, to create 3D $Au−TiO_2$ networks.[38] The similar dimensions of the TiO_2-host particles (~10−15 nm covalently bonded nanoparticles that comprise the networked support) and Au-guest particles (~5−6-nm metal nanoparticles) enables individual Au particles to form multiple interfacial contacts with the surrounding titania support (Figure S1, Supporting Information). This extended multidimensional metal−oxide interface promotes oxidative catalysis of carbon monoxide at Au particles normally considered too large to catalyze the reaction.[38]

The photocatalytic oxidation of methanol is one of the most suitable model reactions to develop a fundamental understanding of the mechanisms of photoassisted and photocatalytic processes.[7] Recently, it was shown that photooxidation of methanol is a hole-mediated process and methoxy, not molecular methanol, is the effective hole scavenger in photochemical reactions of methanol on both single crystal[39−41] and powder[42] rutile TiO_2. In the present study, we investigate the photooxidation of methanol at both TiO_2 and $Au−TiO_2$ aerogels and contrast the results at networked TiO_2 to unnetworked nanoparticulate titania (P25 TiO_2). Liquid-phase photooxidation of methanol has been studied extensively on a number of aerogel materials, including TiO_2 and $TiO_2−SiO_2$,[43] and Au/TiO_2,[26] but there are few spectroscopic studies that have explored how the mechanism may change on 3D mesoporous materials or at TiO_2-supported plasmonic Au particles.

We couple high-vacuum studies to in situ surface-sensitive transmission infrared (IR) spectroscopy to study the real-time adsorption and photooxidation of methanol as the mesoporous materials are irradiated by UV or visible light. The utility of IR spectroscopy in semiconductor photochemistry stems from its ability to simultaneously probe both the discrete vibrational transitions of surface adsorbates and the electronic population within or close to the continuum of the semiconductor conduction band. Our experiments show that the initial uptake of methanol at 3D TiO_2 and $Au−TiO_2$ aerogels is governed by dissociation to methoxy adsorbates within both systems and that UV irradiation of the porous solids efficiently oxidizes methoxy species to surface-bound formates. More importantly, we find that networked-entrained Au particles sensitize the oxide nanoarchitecture and activate it toward photochemistry that extends well into the visible range with photooxidation rates at 550-nm irradiated $Au−TiO_2$ that nearly match those at the UV-irradiated TiO_2 aerogel.

2. EXPERIMENTAL SECTION

2.1. TiO_2 and $Au−TiO_2$ Preparation and Characterization. $Au−TiO_2$ composite aerogels were synthesized in a manner described by Pietron et al.; a weight loading of 5% Au was chosen.[38] First, monolayer-protected gold colloids (Au MPCs) were prepared as previously detailed by Brust et al.,[44] where $AuCl_4^-$ is reduced in the presence of alkanethiolate ligands. The Au MPCs consist of 2−3-nm Au cores protected from aggregation by alkanethiolate monolayers. Mixed-monolayer MPCs can be created by partially exchanging alkanethiolate ligands with a ligand of choice.[45−47] We chose a mixed-ligand monolayer consisting of 2:1 decanethiol and 11-mercaptoundecanoic acid in order to render the MPCs highly soluble in the ethanolic solvents used in sol−gel chemistry, yielding well-dispersed Au in $Au−TiO_2$ aerogels, even after calcination at high temperatures (*vide infra*).

Titania aerogels (with and without incorporated Au) were prepared in a manner similar to that described by Dagan and Tomkiewicz.[48] Briefly, 2.5 g (8 mmol) of titanium(IV) isopropoxide (Alfa Aesar) in 4 g of ethanol was added to a stirred mixture of 0.36 g of H_2O (20 mmol)/3.9 g of ethanol (1:12 v/v) and a catalytic amount of 70% nitric acid (0.7 mmol), yielding a firm gel in minutes. In $Au−TiO_2$ aerogel syntheses, we used the same procedure as for TiO_2 synthesis, but first dissolved mixed-monolayer Au MPCs in the ethanol used in the TiO_2 gel synthesis. The final weight fraction of gold in the $Au−TiO_2$ aerogels was controlled by the ratio of Au MPCs to titania precursor in the solution. In the present study, we used a Au MPC/Ti precursor ratio that produced a final Au/TiO_2 ratio of 5 wt %.

Gels were subsequently aged for 24 h, rinsed with acetone 12 times over 3 days, and loaded under acetone into a supercritical dryer (Fisons Bio-Rad E3100). The gels were rinsed with liquid CO_2 before taking the liquid CO_2 above its critical temperature and pressure (T_c = 304 K, P_c = 7.4 MPa), followed by slowly venting to atmospheric pressure. The amorphous as-prepared composite samples were calcined at 723 K for $Au−TiO_2$ and 698 K for TiO_2 aerogels for 4 h to crystallize amorphous titania to anatase TiO_2 and to combust the alkanethiolate ligands. As

dx.doi.org/10.1021/jp312583w | J. Phys. Chem. C 2013, 117, 15035−15049

reported previously, the calcined Au−TiO_2 aerogels comprise interconnected ∼12-nm anatase nanoparticle networks, with the 2−3 nm Au cores coarsening to ∼5−6 nm Au particles that are integrated into the TiO_2 network.[38] The TiO_2 aerogels are white after calcination, while the Au−TiO_2 composite aerogels are deep purple.

The aerogels were characterized for Brunauer−Emmett−Teller (BET) specific surface area and porosity using nitrogen physisorption measurements (Micrometrics ASAP 2010 accelerated surface area and porosimetry system). Pore size distributions were calculated using Micromeritics DFT Plus software using the Harkins and Jura model[49] and assuming a cylindrical pore geometry.

A third sample of TiO_2, obtained commercially (Degussa P25) and created by the Aerosil process[50] (i.e., via flame hydrolysis), was used as a standard in this work for comparative studies. The P25 TiO_2 is nanoparticulate, composed of 80% anatase (average size 25 nm) and 20% rutile (33-nm average diameter) with a surface area of 50 m^2 g^{-1}.[51]

2.1.1. Physical Characterization of Aerogel Materials. Transmission electron microscopy (TEM) analyses were conducted in dark-field mode at an accelerating voltage of 200 kV (JEOL FasTEM 2010 HR TEM). Aerogel samples were prepared on carbon-coated copper grids by dispersing fine powders in acetone using sonication, followed by depositing a drop of solution onto the grid and evaporating the acetone. The micrographs reveal that the Au−TiO_2 aerogels feature a moderate distribution of Au nanoparticle diameters (d) centered at 4.7 nm (Figure S2A, C, Supporting Information), as observed previously.[38] A series of through-focus transmission electron images (not shown) confirmed, as previously reported, that each Au particle within its 3D reaction volume contacts multiple TiO_2 networked nanoparticles to enhance the number of metal−oxide interfacial junctions (Au||TiO_2) throughout the nanostructured mesoporous material.

X-ray diffraction (Rigaku SmartLab, operated at 40 kV and 44 mA) was used to identify crystal-phase formation after calcination. The Scherrer equation was used to estimate average TiO_2 particle size using the full-width at half-maximum of the anatase (101) reflection at 2θ = 25.5. The XRD measurements reveal only anatase crystalline features for both the TiO_2 and Au−TiO_2 aerogels with no XRD-discernible presence of the rutile habit (Figure S2B, Supporting Information), as was observed previously for materials synthesized and processed in the same manner.[38] The Au(111) and Au(200) reflections are also clearly visible in the diffraction pattern for the Au−TiO_2 aerogel, while the anatase reflections are identical to those for the TiO_2 aerogel host (Figure S2B, Supporting Information).

A BET analysis of the nitrogen physisorption data (not shown) yields a specific surface area of 150 m^2 g^{-1} for TiO_2 aerogel and 138 m^2 g^{-1} for Au−TiO_2 aerogel, as well as comparable porosity of 63.9% and 64.2%, respectively. The two sets of aerogels were calcined at different temperatures (698 and 723 K, respectively), which may explain the ∼10% lower surface area for the Au−TiO_2 aerogel, but TiO_2 aerogels (with and without incorporated Au) calcined at these temperatures typically vary in BET surface area from ∼130 to 180 m^2 g^{-1}, depending on such factors as the purity of the precursor and ambient humidity during the sol−gel synthesis, so this difference is likely due to normal sample variability rather than the slightly higher calcination temperature. Pore size distributions for the two materials are also similar (Figure S2D, Supporting Information, calculated from the N_2 desorption isotherms), yielding an average pore width of 8.8 nm for the TiO_2 aerogel and 10.1 nm for Au−TiO_2.

X-ray photoelectron spectroscopy (XPS) was used to confirm the weight loadings of gold in the composites (Thermo Scientific K-Alpha X-ray photoelectron spectrometer with monochromatic Al Kα X-ray source at 1486.6 eV). The measurements were made using a nominal spot size of 0.1 mm^2, a flood gun (to prevent charging of insulating samples), a step size of 0.15 eV, and a dwell time of 0.1 s. Spectra were recorded in fixed analyzer transmission (FAT) mode with a pass energy of 20 eV; 10 scans were accumulated for the Au 4f and Ti 2p regions. The spectra were then background-subtracted using a Shirley model, analyzed with Unifit 2009 software (University of Leipzig) using Scofield sensitivity factors for Al, and curve-fit using a 70% Gaussian−30% Lorentzian line shape. The integrated intensity for the Au $4f_{7/2}$ and Ti $2p_{3/2}$ peaks was used to quantify the relative atomic percentage of each element. The Au/Ti atomic ratio of Au−TiO_2 aerogel (data not shown) yields a fractional gold loading of 5.1 wt % (wt Au/wt Au−TiO_2), matching the 5 wt % loading targeted during sol−gel synthesis. Because the Au−TiO_2 aerogels are highly porous and inherently nanoscale, XPS can adequately approximate their bulk composition.

Reflectance data derived for the aerogels from diffuse reflectance UV−visible spectra (Perkin-Elmer 750 spectrophotometer with an integrating sphere) were converted to absorption values using the Kubelka−Munk transformation (Figure S3, Supporting Information).

2.1.2. Experimental Set-up and FTIR Spectroscopy. The experimental setup has been described previously;[52,53] only a brief overview will be provided here. The powdered aerogels were pressed into the openings of a tungsten support grid (0.0508-mm thick, with 0.22-mm^2 square openings) as circular spots, 7 mm in diameter. The TiO_2 sample and the Au−TiO_2 sample were mounted on the same grid. An empty region of the grid was used as a spectral reference and for analysis of the gas-phase products. The grid could be resistively heated, and a type-K thermocouple spot-welded to the top center of the grid was used to monitor and regulate the temperature of the samples to within ±1 K. The tungsten grid was suspended in the center of a turbomolecular-pumped stainless-steel vacuum chamber (base pressure 10^{-8} Torr) where it was intersected by the light from a commercial infrared spectrometer.[52,53] The samples could be analyzed by translating the desired region of the grid in-line with the IR beam path. The grid was oriented at 45° with respect to both the IR and the photoexcitation (UV or visible) beams. Infrared spectra were recorded (employing an LN_2-cooled MCT detector) with a resolution of 4 cm^{-1}. Typically, 500 scans were averaged for each spectrum for the steady-state measurements, while 100 scans were averaged for the spectra recorded during methanol adsorption and under dynamic pressure regimes.

Although the absolute surface areas of the grid-supported pressed samples used for the IR studies have not been explicitly measured, the TiO_2 aerogel, the Au−TiO_2 aerogel, and the commercial P25 standard sample all exhibit similar coverages when the surfaces are saturated by methanol or carbon monoxide adsorbates (see below). Our measurements indicate that the relative surface areas of the prepared samples employed throughout this work are the same to within a factor of 1.2.

The high-vacuum stainless-steel gas line had a calibrated volume that was used to dose either methanol, CO, or O_2; gas pressure was measured by a capacitance manometer. The

methanol (Aldrich, 97%) was stored in a 20-cm^3 glass bulb connected to the gas line and purified via five freeze−pump−thaw cycles. The oxygen (99.999%; Airgas, Inc.) and CO (99.999%; Airgas, Inc.) were used without further purification.

2.1.3. Sample Activation and Saturation with Methanol. *2.1.3.1. Activation.* The samples were heated under vacuum in the reaction chamber in 50-K intervals from 295 to 675 K and held at each temperature step for 30 min under vacuum. During thermal activation, the organic contaminants on the aerogel surfaces desorbed or combusted; the samples were then oxidized at 675 K by exposure to 20 Torr of pure oxygen for 60 min, followed by evacuation at the same temperature for 10 min. The samples were re-exposed to O_2 at 20 Torr and 675 K for 10 min, evacuated at 473 K for 10 min, and cooled to room temperature under vacuum; the infrared signature verified that the samples were reoxidized.[54,55] As expected from previous studies,[56,57] the activation of Au−TiO_2 and TiO_2 samples by vacuum annealing and oxidation with O_2 at 673 K removed most of the organic residue that remained following the sol−gel preparation procedure, as shown by spectra a and a′ in Figure S4A, B, Supporting Information. Prior to methanol exposure, the samples were heated at 500 K for 30 min under vacuum (1×10^{-7} Torr) to remove adsorbed background gases from the surface. During this procedure, an LN_2-cooled cryoshield was employed to remove water and other condensable gases from the chamber.

2.1.3.2. Saturation. The samples were saturated with methanol at 295 K by stepping to successively higher pressures (0.2 to 2 Torr) with the cryoshield maintained at liquid-nitrogen temperature to trap water and other gases. Once the particles were coated with adsorbed methanol, the system was evacuated, and the cryoshield was warmed. This procedure minimizes the water-vapor concentration in the chamber. The IR spectra for each sample recorded during methanol uptake indeed show no evidence of residual surface water contamination (see Figure S5, Supporting Information).

2.2. Photochemistry by UV and Visible Irradiation. By the prior protocol,[58] the photochemistry of surface-adsorbed methanol at 295 K was examined by first saturating the surface with methanol vapor, evacuating residual methanol from the chamber, and then irradiating the samples under both anaerobic (vacuum) and aerobic (20 Torr O_2) conditions. For both UV and visible irradiation, the same light source was employed: a high-pressure 350-W mercury arc lamp (Oriel Corp.) equipped with a water filter to remove IR radiation. The intensity of the UV radiation measured at the sample position was 200 mW cm^{-2}. To limit the photoexcitation energy to values slightly above the band-gap energy (3.2 eV for anatase), a long-wave pass cut-on filter (Newport Corp. 20CGA-345; λ = 345 nm, 3.59 eV) was used for the UV-exposure experiments. For visible irradiation, three bandpass filters (70 nm full-width at half-maximum transmission profile) were used with peak transmissions centered at 400, 500, or 550 nm.

3. RESULTS AND DISCUSSION

To explore the thermal and photochemical reactivity of the 3D mesoporous TiO_2 and TiO_2-supported Au networked materials, we chose methanol as the test reactant because it is a common product of the oxidation of more complex species[56] yet is simple enough structurally that its surface chemistry can be tracked with conventional infrared spectroscopic methods. The 3D aerogels were designed to provide high surface area and extreme stability in the harsh conditions often required to achieve efficient heterogeneous catalysis. The 3D covalently bonded TiO_2 networks significantly stabilize metallic Au particles against thermal migration, provide open pathways for mass transport to and from the active centers, and significantly increase the number of metal−semiconductor junctions where charge transport and surface chemistry may occur.

3.1. Dissociative Adsorption of Methanol. Following thermal activation of P25 TiO_2 and Au−TiO_2 and TiO_2 aerogels, we tracked the dynamics of adsorption by exposing the samples to methanol vapor while recording infrared spectra at varying time intervals. In general, we find that the IR spectral features for the methanol-saturated aerogels and P25 TiO_2 are nearly identical in terms of the energies of many of the modes, but the Au−TiO_2 aerogel differs significantly in the relative intensity of key peaks compared with the two TiO_2 materials (Figure 1A, B). From the peak positions, one may conclude

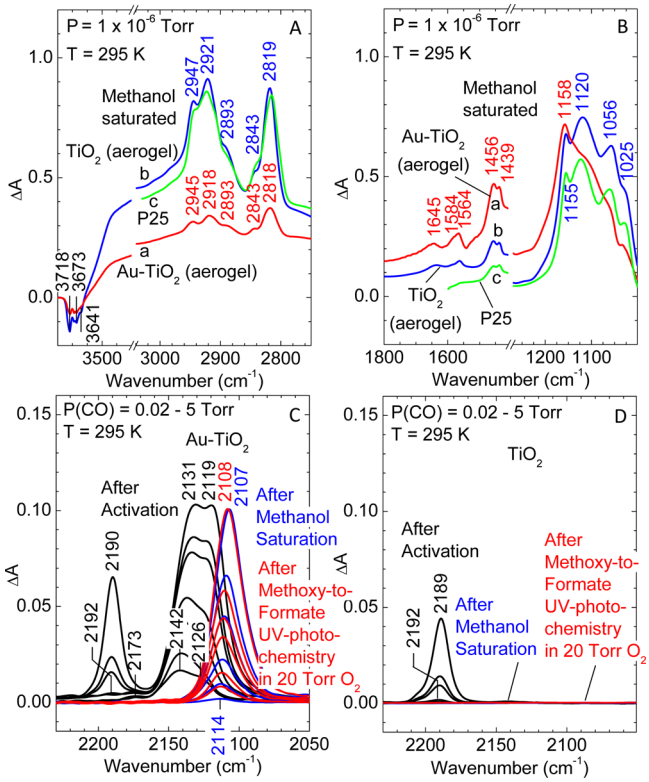

Figure 1. (A, B) Dissociative adsorption of methanol on clean Au−TiO_2 (red) and TiO_2 (blue) aerogels and on Degussa P25 TiO_2 (green). Difference IR spectra obtained in high-energy (A) and low-energy (B) regions after saturation with methanol (see Figure S5, Supporting Information, for the dynamics of IR spectra with surface methanol coverage). (C, D) Characterization of Au and Ti surface sites via CO(a) vibrational frequency at increasing CO gas pressures from 0.02−5 Torr at 295 K for (C) Au−TiO_2 and (D) TiO_2: (black) methanol-free surfaces; (blue) methanol-saturated surfaces; (red) spectrum for CO adsorption following UV irradiation of the methanol-saturated surface. The spectra are normalized for sample loading.

that the chemical identity of the adsorbates at both aerogel surfaces are similar to those that form at P25 titania, which is in accord with previous studies of methanol chemistry on nonaerogel Au/TiO_2[59,60] and TiO_2.[57,60−64] The previous work involving methanol uptake on nanoparticulate titania suggests that the adsorption mechanism is dominated by

dx.doi.org/10.1021/jp312583w | J. Phys. Chem. C 2013, 117, 15035−15049

dissociation through protonation of the titania and formation of surface-bound methoxy groups. The key modes that indicate extensive methoxy formation on Au−TiO_2 appear at 2918 and 2818 cm^{-1} (Figure 1A, spectrum a) and at 2921 and 2819 cm^{-1} for TiO_2 (Figure 1A, spectrum b), which are due to the asymmetric $\nu(CH_3)_a$ and the symmetric $\nu(CH_3)_s$ modes of methoxy groups, respectively. The adjacent small bands at 2945 and 2843 cm^{-1} for Au−TiO_2 (spectrum a) and at 2947 and 2843 cm^{-1} for TiO_2 (spectrum b) are assigned to the corresponding $\nu(CH_3)_a$ and $\nu(CH_3)_s$ modes of molecularly adsorbed methanol.[57,60,62,63,65−68] The small shoulder at 2893 cm^{-1} that appears with both samples (spectra a and b) is due to the overtone of the $\delta(CH_3)$ deformation mode in Fermi resonance with $\nu(CH_3)$ vibrations.[69]

In addition to the C−H stretching region, the spectra in the low-frequency region (Figure 1B) provide additional information about the bonding of methanol and methoxy species to the Au−TiO_2 and TiO_2 surfaces. The small bands that appear at 1645 and 1584−1564 cm^{-1} [$\nu_{as}(OCO)$] are assigned to carboxylate-type species, most likely formates,[57,60] produced via limited conversion of methoxy groups. Consistent with previous results,[56] the thermal conversion of methoxy groups to formates appears to occur more readily on the surface of the Au−TiO_2 sample. The bands at 1456 and 1439 cm^{-1} are attributed to the $\delta(CH_3)$ modes of methoxy groups, and the three bands at 1120, 1056, and 1025 cm^{-1} are assigned to the $\nu(OC)$ modes of methoxy groups in single-, double-, and triple-bond configurations to Ti sites.[57−59,67,70]

Although the $\nu(OC)$ modes appear at nearly identical wavenumbers for the two aerogel samples (Figure 1B and Figure S5, Supporting Information), they exhibit substantially different intensities on the Au−TiO_2 and the TiO_2 aerogels (Figures S5 and S6, Supporting Information). Assuming identical absorptivities for the $\nu(OC)$ modes, one finds that the monodentate methoxy groups (1120 cm^{-1}) are the dominant surface species on both materials, while the doubly (1056 cm^{-1}) and triply (1025 cm^{-1}) bound methoxy groups account for less than a quarter of the species (Figures S5 and S6, Supporting Information). The band that appears at 1155 cm^{-1} in the spectrum of both Au−TiO_2 and TiO_2 aerogels at low methanol coverage was previously assigned to the rocking mode of methyl groups.[57,70] At the highest methanol/methoxy coverages for the Au−TiO_2 sample, this band gains substantial intensity and shifts to 1158 cm^{-1} (Figures S5 and S6, Supporting Information), hinting that this O−CH_3 mode is energized at the adsorption site on Au−TiO_2. Boccuzzi et al.[59] tentatively assigned a similar band in their studies of methanol adsorption to an on-top methoxy species on Ti^{3+} adjacent to both an oxygen vacancy and metallic gold at the border of a Au||titania interfacial junction. The spectrum of the methanol-saturated Au−TiO_2 sample obtained in this work (Figure 1B; Figures S5 and S6, Supporting Information) clearly shows that the intense band at 1158 cm^{-1} is related to the presence of Au particles, which suggests that this mode, in agreement with the previous assignment,[59] is due to on-top methoxy adsorbates adjacent to the Au−titania interface.

3.2. Characterization of Au and Ti Surface Sites via CO(a) Vibrational Frequency. Although the mode assignments described above provide insight into the likely surface adsorbates, they reveal little information about the nature of the surface site where the chemistry occurs. Therefore, we used surface-adsorbed CO to help characterize the sites responsible for methanol uptake. Surface-adsorbed CO exhibits a strong vibrational frequency dependence on the electron-donating character of the site to which it binds.[71−79] The effect is due to hybridization of the CO orbitals with the surface states, which shifts the CO vibrational mode to lower frequency when the π-system interacts strongly or to higher frequency for σ-interactions between the CO and the surface.[71,80]

Figure 1C, D summarizes the results of the spectroscopic studies after adsorbing CO at increasing CO pressures from 0.02 to 5 Torr (at 295 K) at clean and methanol-saturated mesoporous Au−TiO_2 and TiO_2 aerogels. On both clean Au−TiO_2 and TiO_2 aerogel surfaces, adsorption of CO on the TiO_2 regions produces a band at 2192 cm^{-1} that only slightly shifts to lower wavenumber with increasing CO pressure. This band is attributed to CO bound to coordinatively unsaturated (CUS) Ti sites that act as Lewis acid centers. That is, binding of CO to cationic surface sites reduces the antibonding character of the 5σ level of CO (centered primarily on the carbon atom),[80] thus increasing the overall bond order of the molecule[71] and significantly blue-shifting the $\nu(CO)$ stretching mode by 49 cm^{-1} with respect to gas-phase CO. This behavior supports the existence of strong Lewis acid sites on the anatase TiO_2 nanoparticles that comprise the aerogel network, as previously observed for CO adsorption on isolated anatase TiO_2 particles.[81−84] The frequency of this high-energy Ti−C═O mode (~2190 cm^{-1}) is nearly identical for both Au−TiO_2 and TiO_2 aerogels (Figure 1C,D, respectively) and the shape of the band is largely insensitive to CO pressure.

While the simple spectrum for the TiO_2 aerogel indicates that CO binds nearly exclusively to a single CUS Ti site, the absorption spectrum for CO on the Au−TiO_2 aerogel surface is much more complex (contrast panel C with panel D in Figure 1). Most notably, the IR spectrum of CO adsorbed at the activated Au−TiO_2 sample (Figure 1C) exhibits two strong bands at 2142 and 2126 cm^{-1} that appear at low CO equilibrium pressure (0.02 Torr) and dominate the spectrum throughout the entire coverage regime. Both bands rise in intensity and shift systematically to lower frequency with increasing CO coverage and appear at 2131 and 2119 cm^{-1}, respectively, at 5 Torr equilibrium CO pressure. The high-frequency bands observed at low coverage (2142−2131 cm^{-1}) are attributed to a $Au^{\delta+}CO$ species.[42] Positively charged gold atoms ($Au^{\delta+}$) involved in Au−O−Ti linkages are posited to form at the metal−support interface around the perimeter of the gold nanoparticles. Similar vibrational frequencies for CO adsorbed at $Au^{\delta+}$ sites appear following Au/TiO_2 surface oxidation[42,72,74,85−89] when active oxygen species are available at the Au particle periphery or as adatom oxygen on the surface of the particles. The existence of $Au^{\delta+}$ surface sites at the titania−gold interface may help explain the high activity for CO oxidation at these 3D continuous mesoporous networks.[38] As recently reported, molecular oxygen is activated at dual Ti_{5c}/Au interface sites (Ti_{5c} refers to 5-fold Ti sites) and dissociates via assistance of neighboring $Ti_{5c}CO$ species.[89] The lower-frequency bands (2126−2119 cm^{-1}) observed as coverage increases on the clean surfaces are assigned to a $\nu(Au^0CO)$ mode that arises from bonding of CO to low coordinated neutral Au^0 gold sites that form at Au steps (edge Au atoms),[90,91] in agreement with experimental[42,72,74,76,79,87,91−97] and theoretical work.[91,96]

Figure 1C, D shows that CO binds very differently to the two materials when they are presaturated with methanol. The $\nu(Au^0CO)$ mode for CO at low coordinated neutral gold sites (Au^0) appears at 2114−2108 cm^{-1} on the surface of methanol-

dx.doi.org/10.1021/jp312583w | J. Phys. Chem. C 2013, 117, 15035−15049

saturated Au−TiO_2, while no CO adsorption is detected at the methanol-saturated TiO_2 aerogel (Figure 1D).[57] The inhibition of CO adsorption by preadsorbed methanol/methoxy groups is attributed to the ability of methanol to block the CUS Ti sites (the Lewis acid centers). That is, as a weaker base, CO cannot displace either methanol or methoxy adsorbates.[57]

On the basis of the above spectral data, along with previous experimental[39,57,60,62−67,98] and theoretical[99−103] results, we hypothesize that the CUS Ti sites on mesoporous anatase play the role of active Lewis acid centers where methanol adsorbs and dissociates to protonate the surface and produce surface-bound methoxy species, Ti^{4+}_{5c}−OCH_3. The XRD data (Figure S2B, Supporting Information) indicate that (101) is the primary reflection for both TiO_2 and Au−TiO_2 materials, suggesting that the equilibrium structure is dominated by the anatase (101) crystal plane. The thermodynamically most stable TiO_2 surfaces are anatase (101) and rutile (110). It is well established that nanoscale anatase and rutile powders possess a large percentage of (101) and (110) surfaces, respectively.[104] On the surface of anatase, the role of CUS Ti sites is played by 5-fold Ti (Ti_{5c}) sites that are exposed on both the highly stable (less reactive) (101) surface and the less stable (more reactive) (001) surface.[99] However, calculations show that molecular adsorption of methanol dominates on the stoichiometric TiO_2(101) surface,[103] while dissociative adsorption is favored on the clean TiO_2(001) surface at both low and high methanol coverages.[99] The high reactivity of the anatase (001) surface is attributed to active 2-fold O (O_{2c}) sites: CH_3O binds to Ti_{5c} while H binds to a nearby O_{2c} as the Ti_{5c}−O_{2c} bond ruptures.[99] Therefore, although the majority of the particles in the system studied here are characterized by (101) geometries, the extensive methanol dissociation on the TiO_2 and Au−TiO_2 aerogels may be due to the presence of highly reactive anatase (001) surface structures.

The methoxy adsorbates are stable on anatase TiO_2 surfaces that are remote from Au||TiO_2 interfaces, but they appear to convert to carboxylate type species at sites near the Au nanoparticles in the Au−TiO_2 aerogel. This reaction likely occurs at the periphery of the gold particles, because Au−O−Ti linkage sites are strongly oxidizing.[38,56,89] Other researchers have demonstrated that these same sites are likely the regions where CO oxidation occurs on Au/TiO_2 nanoparticulate systems.[89] As the methanol is oxidized, the gold is reduced, which is evidenced by the disappearance of IR signal for the $\nu(Au^{\delta+}CO)$ modes.

3.3. Dynamics of Photoinduced Charge Generation. Following the studies of methanol uptake, we explored the UV- and visible-light-induced generation of charge carriers in both TiO_2 and Au−TiO_2 methanol-saturated aerogels by recording infrared spectra in situ with light irradiation. Numerous previous studies have highlighted the significant utility of IR spectroscopy as an effective probe of both free conduction band (CB) and delocalized shallow-trapped (ST) electrons in photoexcited TiO_2.[54,105−107] As occurs with the high-energy photon sources used to study band structure in semiconductors, IR photons can induce electronic transitions, provided the electrons are trapped in shallow states just below or within the conduction band.

Figure 2 summarizes the IR spectra recorded for methanol/methoxy-saturated nanoparticles during irradiation with either broadband UV−vis (λ > 350 nm) or narrow-band visible-light (λ = 550 nm). The spectra obtained after 60 min of UV irradiation (Figure 2A, B) show a significant increase in the

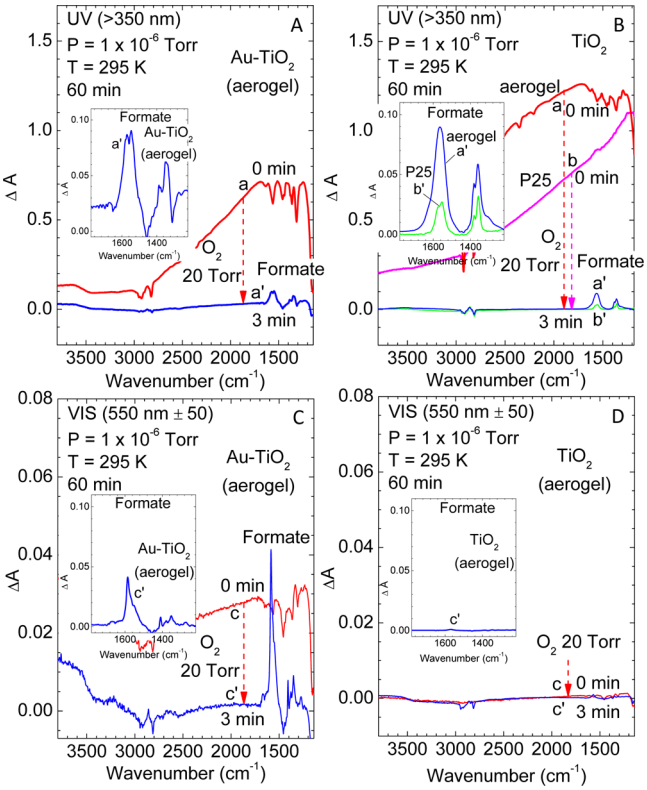

Figure 2. The IR electronic spectrum of methanol-saturated Au−TiO_2 and TiO_2 aerogels and P25 TiO_2 samples after 60 min of photoexcitation with UV (A, B) and visible (C, D) light (red); quenching of the IR electronic spectrum by exposure to O_2 gas (blue). The spectra are normalized for sample loading.

background absorbance across the entire spectrum, with a maximum at ~1700−1100 cm^{-1}. This prominent IR absorption has an electronic origin that reflects the composite effect of two distinct optical processes: the indirect acoustic phonon-mediated intraband infrared excitation of free CB electrons[54,105−107] and the direct interband infrared excitation of ST electrons.[54] Similarly strong IR absorbance due to electronic excitations was observed recently with methanol/methoxy-saturated rutile nanoparticles during UV excitation under analogous conditions.[58]

The energy of the UV irradiation used in these experiments (3.54 eV at λ = 350 nm) exceeds the 3.2-eV band-gap energy for anatase TiO_2. Irradiation of semiconductor TiO_2 nanoparticles with UV light at energies exceeding their band gap generates mobile charge carriers that populate the conduction band and valence band (VB) of the particles. The majority of these charge carriers undergo fast (within nanoseconds) direct nonradiative electron−hole pair recombination. Some of the charge carriers undergo radiative recombination, while a fraction of the electron−hole (e^-−h^+) pairs avoid recombination because they become trapped within various states.[2,3,107−109]

Methanol has been identified in numerous previous studies as an efficient hole scavenger on TiO_2.[7,39,110−112] Importantly for our work, Shen and Henderson[39] have recently shown that surface methoxy groups are effective hole scavengers in methanol photochemistry on rutile TiO_2(110). On the basis of this precedence, we attribute the significant lifetime (even at room temperature) of the photogenerated electrons, demonstrated in Figure 2A, B, to the efficient trapping of

dx.doi.org/10.1021/jp312583w | J. Phys. Chem. C 2013, 117, 15035−15049

photogenerated holes by methoxy adsorbates. The product of this electron transfer reaction is a $Ti^{4+}_{5c}-OC^{\bullet}H_3$ species on the anatase TiO_2 aerogel. Similar observations have been recently reported for methanol adsorbates on rutile TiO_2 nanoparticles.[54] These results agree with recent theoretical predictions,[103,112] which suggest that the interaction of methanol with the TiO_2 surface shifts the methanol HOMO to just below the valence-band edge, making it near-resonant with the UV-generated holes. DFT calculations have shown that the methanol/methoxy O-2p valence states may be −0.5/−0.4 eV below the valence-band maximum (VBM) of TiO_2.[112] This electronic shift accounts for the efficient hole-trapping character of adsorbed methanol. Moreover, the high-energy band for terminally adsorbed methoxy groups is even closer to the VBM than for bridging methoxy groups, which may account for the previously observed photoactivity of the surface-bound methoxy groups.[103,113]

Once holes are trapped at the surface, the methoxy radicals obtain a partial positive charge, which polarizes the interface to produce an electric field at the surface of the semiconductor. The electric field effectively repels additional positive holes from the surface while attracting negative electrons, similar to the well-known band-bending effects caused by surface adsorbates.[21] Such band bending leads to efficient electron−hole-pair separation and reduces the rate of recombination, thereby enabling observation by IR spectroscopy. While the nature of the band bending that occurs in the networked nanoparticles comprising the aerogels is expected to be different in magnitude and length scale than that described for extended bulk materials, the rate of e^+-h^- recombination appears to be reduced by charge trapping at the surface, which polarizes the interface and thus facilitates charge migration.

The integrated electronic absorbance, that is, the concentration of accumulated CB and ST electrons, in the UV-irradiated TiO_2 aerogel (Figure 2B, spectrum a) is a factor of 1.6 larger than that observed for the anatase/rutile TiO_2 P25 sample (Figure 2B, spectrum b) and a factor of 2 greater than that measured on the Au−TiO_2 aerogel sample (Figure 2A, spectrum a). The larger excited-state electron density in the irradiated TiO_2 aerogel relative to that in P25 TiO_2 is most likely due to the connectivity of the 3D network. Networking in nanoscale TiO_2 has elsewhere been shown to facilitate electron−hole separation. For example, separation of charges with quantum efficiency as high as 46% was recently reported for UV-irradiated wet titania gels.[114] In addition, networked mesoporous TiO_2 aerogel photoanodes exhibit higher steady-state CB electron density (32% more) and longer lifetime (by a factor of 2) compared with P25 TiO_2-based electrodes.[115]

In contrast to the extended lifetime of CB electrons in the pure TiO_2 aerogel, the Au−TiO_2 aerogel exhibits weak IR signal due to accumulated electrons (Figure 2A). The smaller population of CB and ST electrons for the Au−TiO_2 aerogel may be due to the existence of defect sites created near the Au‖TiO_2 interfacial contacts. Defect sites, like oxygen vacancies, can serve as deep electronic traps or as charge recombination centers, both of which serve to decrease the number of IR-active electrons in Au−TiO_2. Photoexcited electrons may also be rapidly transferred from the CB of TiO_2 into Au nanoparticles, thus becoming transparent toward the IR radiation. The driving force for potential electron transfer is the difference in the Fermi level of photoexcited TiO_2 and ground-state Au particles.[7,21,116]

As expected,[117] upon decreasing the energy of the photoexcitation radiation to ∼2.5 eV (λ = 550 nm), well below the band-gap energy of anatase, no interband transitions occur in the TiO_2 aerogel and consequently no rise in the IR background absorbance occurs (Figure 2D, spectrum c; see also Figure S7B, spectrum c, Supporting Information). The Au−TiO_2 aerogel, however, exhibits a broadband rise in the background absorbance upon irradiation at 550 nm (Figure 2C, spectrum c), which is attributed to free CB and ST electrons that accumulate in the TiO_2 component of the methanol-saturated Au−TiO_2 aerogel. The excited electrons in the anatase TiO_2 component of the Au−TiO_2 system most likely result from a visible-light-induced surface plasmon resonance in the Au nanoparticles, which has a broad peak centered at 550 nm, as revealed in the diffuse-reflectance spectrum (Figure S3, Supporting Information).

Previous studies have established that light-induced plasmons produce strong effects in both the near- and far-field response of Au nanoparticles.[20] Essentially, the role of a localized surface plasmon is to concentrate the energy of incoming photons in small volumes surrounding the plasmonic nanostructure.[16] The photophysical mechanisms responsible for surface plasmon resonance induced charge generation in metal−semiconductor nanostructures remain a subject of intense experimental and theoretical studies. Although uncovering the photophysical mechanism of visible-light electronic excitation in the Au−TiO_2 aerogel is beyond the scope of the current study, several excellent reviews of these mechanisms have recently appeared in the literature.[6,16,20,22,23]

3.4. Photochemistry: TiO_2 and Au−TiO_2 Aerogels under Anaerobic Conditions. In addition to revealing methanol hole-trapping and electronic excitation within both aerogel samples, the spectra labeled a in Figure 2A, B exhibit significant negative features that correspond to a decrease in absorptivity of the methoxy and methanol modes on the surface. Although these negative features appear to be due to decomposition of the surface adsorbates during photonic irradiation, the modes quickly recover when the excited electrons are quenched by adding oxygen into the chamber. Oxygen scavenges energetic electrons in titania,[5,58,104,107,118] which immediately returns the broad electronic absorbance to zero. As shown by spectrum a′ in Figure 2A and spectra a′ and b′ in Figure 2B, oxygen almost completely returns the IR difference spectrum to the original baseline, but this change is accompanied by the sharp negative features in the CH stretching region becoming much less prominent. (Note that the UV excitation was performed under vacuum, where readsorption of background gases is minimal.) The nearly complete disappearance of the negative IR modes upon depletion of excited electrons by O_2 suggests that these negative features are due to electric-field changes within the particles, rather than significant chemical reactions (or desorption) on the surfaces. Such behavior was also observed with methanol-saturated rutile nanoparticles under UV excitation in vacuum[58] and was attributed to the trapped-carrier-induced Stark effect.[119−121]

Appearing with the methoxy-derived negative features are positive features at 2868 and 1570 cm^{-1}, along with a doublet at 1370 and 1360 cm^{-1} (Figure 2A, spectrum a′, and Figure 2B, spectra a′ and b′), which are assigned to the production of surface-bound formates[58,60,122−124] created on Au−TiO_2 and TiO_2 aerogel and P25 TiO_2 samples during UV excitation. The very similar relative intensities of the formate modes at both

dx.doi.org/10.1021/jp312583w | J. Phys. Chem. C 2013, 117, 15035−15049

aerogel samples (see the insets in Figure 2A, B) show that the pure anatase TiO_2 and Au-loaded TiO_2 3D networks exhibit almost the same activity for methoxy-to-formate conversion under anaerobic conditions during UV exposure. It is also worth noting that the activity of anatase TiO_2 aerogel for formate production is a factor of 4 larger than that of the mixed phase commercial P25 TiO_2 sample under identical conditions (see the inset in Figure 2B). The higher activity of the aerogel sample is likely due to more efficient charge separation that occurs in 3D interconnected particle networks, as previously observed for networked titania sol–gel-derived materials.[114,115]

The understanding that emerges from the data in Figure 2 is that UV irradiation of methanol/methoxy-covered TiO_2 and Au–TiO_2 aerogels primarily leads to the hole-trapping reaction, which effectively accumulates free CB and ST electrons in TiO_2. As recently proposed,[58] a small fraction of the methoxy radicals, produced through this hole attachment reaction, are further oxidized to surface formates. This is the so-called two-electron oxidation process[58,125,126] in which surface methoxy groups are photoconverted to stable surface formate species. The efficiency of methanol oxidation is ultimately destroyed by the accumulation of surface charge,[58] which hinders the migration of the holes that are required for multielectron oxidation.[21,58]

We note that the low-temperature (120 K) hole-mediated photooxidation of surface methoxy to formaldehyde has been reported previously for UV-irradiated rutile TiO_2(110) under anaerobic conditions.[39] In addition, the hole-mediated photocatalytic deprotonation of methanol on TiO_2 surfaces has been critically reviewed in detail.[127] On-going research will continue to elucidate the electron-transfer mechanisms that govern the photocatalytic oxidation of alcohols.[127]

Visible-light irradiation of Au-free TiO_2 aerogel (spectrum c′ in Figure 2D) induces no measurable photochemistry, which is not surprising because the sub-band gap photon energy of ~2.5 eV is insufficient to generate e^-–h^+ pairs.[117] In contrast, low-energy visible irradiation at 550 nm photogenerates charge carriers in methanol-saturated Au–TiO_2 aerogel, as indicated by the small rise in the IR electronic absorbance (Figure 2C, spectrum c) and drives the photochemical decomposition of bound methoxy groups to create surface-bound formates. The photochemical reaction products are revealed in the infrared spectrum upon quenching the excited electrons by oxygen (spectrum c′ in Figure 2C).

The observation that virtually no formate species are produced upon visible-light irradiation of pure TiO_2 aerogel suggests that the hole-driven visible-light photoconversion of methoxy groups at the Au–TiO_2 surface is induced by plasmonic excitation of the Au particles. That is, the observed electron accumulation in the TiO_2 regions of the sample and the formate production at the Au‖TiO_2 interface are likely consequences of effective charge separation in the visible-light-excited Au–TiO_2 aerogel, as recently reported in the transient absorption studies by Du et al.[14,23]

Although the mechanistic details for excitation and separation of e^-–h^+ pairs during visible irradiation of Au–TiO_2 are a topic of intense study and have yet to be elucidated for most systems,[6,16,22,23] our results suggest that charge accumulation at the interface plays a role in limiting both the visible- and ultraviolet-light-induced photochemistry. Therefore, we have repeated the above measurements in the presence of gas-phase O_2, which effectively scavenges excess surface electrons, to explore the UV- and visible-light-driven oxidation of methanol.

3.5. Photochemistry: TiO_2 and Au–TiO_2 Aerogels under Aerobic Conditions. Because we hypothesize that accumulation of surface electrons ultimately limits the extent of two-electron methanol oxidation on the surface, we probed the photochemistry of methanol in the presence of gas-phase O_2, conditions more common to typical photocatalysis. Irradiation of TiO_2 and Au–TiO_2 aerogels with either UV or visible light in the presence of 20 Torr of O_2 much more efficiently produces surface-adsorbed formates (Figure 3) and even

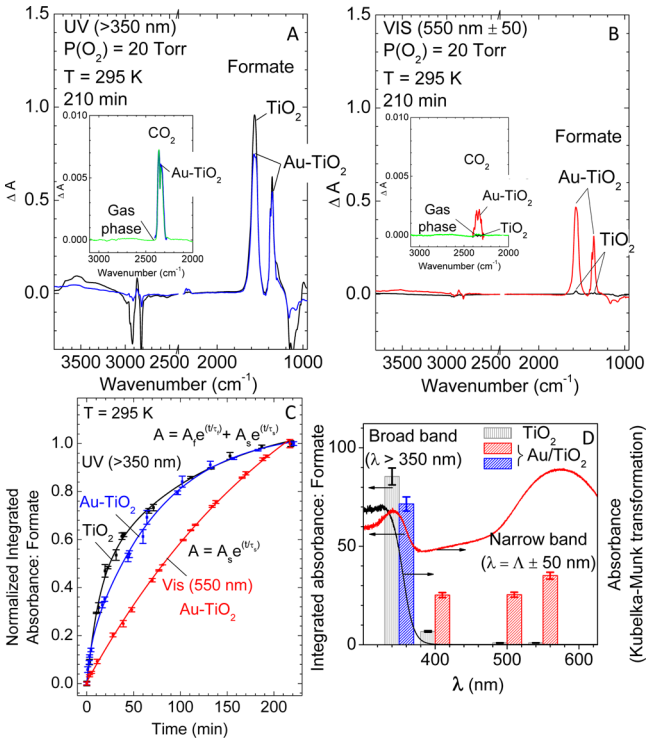

Figure 3. UV (A) and visible (B) light-induced photoconversion of methoxy to formate species on Au–TiO_2 and TiO_2 aerogels under aerobic conditions. (C) Kinetics of formate production during light irradiation of samples. (D) Excitation wavelength dependence of formate production at Au–TiO_2 and TiO_2 aerogels and plasmon resonance absorbance spectrum of the Au–TiO_2 aerogel. The spectra are normalized for sample loading.

demonstrates that a small fraction of the methanol completely oxidizes to CO_2 at Au–TiO_2. Although UV-driven photocatalytic chemistry at TiO_2 aerogels is expected,[43,128–131] these results demonstrate that the same chemistry occurs for low-energy visible-light irradiation when Au particles are present to mediate the transfer of photonic energy into electronic excitations.

3.5.1. UV Photochemistry (Broadband λ > 350 nm). In addition to formates, production of gas-phase CO_2 is also observed during UV excitation of the particles (see inset, Figure 3A). We find that UV photooxidation of methanol on both samples generates identical products under both aerobic and anaerobic conditions; however, the steady-state presence of gas-phase O_2 enables the reaction to proceed more efficiently (Figure 3C) than under the anaerobic conditions discussed above. In the presence of oxygen, the intensity of the IR peaks for the formate groups is over an order of magnitude greater than that under anaerobic conditions (Figure 3A). With oxygen

dx.doi.org/10.1021/jp312583w | J. Phys. Chem. C 2013, 117, 15035–15049

present to scavenge trapped surface electrons that are generated during the two-electron oxidation of methanol, the steady-state population of electrons in anatase TiO_2 particles decreases due to electron transfer to form radical anion oxygen adsorbates on the surface of titania.[110,132] Oxygen and other electron-acceptor adsorbates are known to bend the bands of n-type semiconductors (ZnO, TiO_2, etc.) upward,[21,133,134] which drives hole diffusion toward the surface. Although such band-bending descriptions of the electronics differ on nanostructured materials, oxygen most likely does serve as an electron acceptor on the surface that counters the polarization caused by adsorbed methoxy groups. The overall effect of oxygen may be to enable holes to diffuse back toward the interface where they efficiently oxidize the methoxy groups and provide a reactive pathway for the decomposition of the radical anion $Ti^{4+}_{5c}-OC^{\bullet-}H_2$ intermediate.

This description of the photochemistry is consistent with the recent work by Bahnemann and co-workers[104] who have studied the photocatalytic activities of well-defined single-crystal TiO_2 surfaces toward the liquid-phase photooxidation of methanol to formaldehyde in the presence of dissolved O_2. They showed that the anatase (101) surface has higher photocatalytic activity than rutile (110), (100), and (001) surfaces. Importantly, their results suggested that methanol reacts with $OH^{\bullet}$ radicals or with surface-trapped holes to form a $^{\bullet}CH_2OH$ intermediate and that the dissolved oxygen serves to scavenge conduction-band electrons, which fosters oxidation.[104]

3.5.2. Visible Photochemistry (Narrow-band λ = 550 nm). While the UV-irradiated aerogels exhibit similar formate production rates and infrared spectra, the two samples respond dramatically differently when irradiated with visible light. Photoactivity is nearly completely nonexistent for the anatase TiO_2 aerogel under illumination at 550 nm (Figure 3B), while the Au−TiO_2 aerogel exhibits substantial activity toward methanol-to-formate photooxidation (Figure 3B). As shown in Figure 3D, the formate production on the Au−TiO_2 aerogel during irradiation with 550-nm light is only a factor of 2 lower than that observed with UV exposure under identical conditions. In addition, we note that the kinetics for formate production under UV- and visible-light irradiation, although leading to similar products, appear to be fundamentally different (Figure 3C). Formate production under UV irradiation at both aerogel samples exhibits biexponential dependence, while visible irradiation of Au−TiO_2 exhibits single-exponential dependence. This difference is likely related to the differing mechanisms for e^-−h^+-pair generation and separation and is a topic for future studies.

In addition to narrow-band excitation at 550 nm, we also explored photooxidation at shorter wavelengths (UV, 400 nm, and 500 nm)) under identical conditions of temperature, oxygen pressure, and irradiation time. Formate production decreases dramatically for methanol-saturated TiO_2 aerogel at all excitation wavelengths longer than ∼400 nm (i.e., the low-energy range of UV light) with an order of magnitude lower intensity for formate bands relative to that produced during UV exposure. The photochemistry nearly completely vanishes for 500- and 550-nm excitation (Figure 3D, black hatched bars), as expected because photons at wavelengths longer than 400 nm have insufficient energy to excite electrons within titania. In contrast, the Au−TiO_2 aerogel not only remains active for methanol photooxidation at λ = 400 nm, but formate production efficiency in the presence of oxygen actually increases as excitation energy decreases (Figure 3D, red hatched bars).

Previous studies have established that the wavelength dependence of Au/TiO_2-mediated photocatalytic or photochemical activity closely tracks the UV−visible absorption spectrum for Au/TiO_2.[5,15,17,19,25] In our work, the absorption spectrum of Au−TiO_2 aerogel maximizes at λ = 550 nm due to the formation of a localized surface plasmon and maps onto the photonic excitation energy that leads to the greatest photochemical oxidation activity (See Figure 3D). The coincidence in excitation energy between methoxy-to-formate conversion efficiency and surface plasmon excitation implies that this photoconversion may be governed by local surface plasmon-induced generation of charge carriers in the Au−TiO_2 composite under visible-light irradiation. However, inspection of the 400−500 nm range in Figure 3D shows that the activity measured at 400 nm is slightly higher than that expected for a direct 1:1 correlation to the visible absorption spectrum for this material. Recent work[12,19,135,136] has shown that Au 5d−6sp interband transitions (IBT) play an important role in the optical response of Au nanoparticles. Surface plasmon-assisted d-hole scattering changes the absorption line shape, in terms of both a frequency shift and a broadening at short time delays, in the vicinity of the SPR. However, the enhanced activity at 400 nm in our system is most likely not due to an IBT because coupling of the IBT with the local surface plasmon would be expected to cause rapid damping of the plasmon. Rather, the enhanced activity is likely due to contributions from the TiO_2 component of the material that remain active at 400 nm (see Figure 3C).

Regardless of the specific mechanism for electronic excitation of the TiO_2 during visible-light irradiation, the data from Figure 3 clearly demonstrate photooxidation of methanol in this low-energy excitation range. Upon exposure of Au−TiO_2 aerogel to visible light, formate bands at ∼2859 and ∼1584 cm^{-1} emerge in concert and dominate the spectrum after the initial 15 min of irradiation (Figure 4, upper panels). In addition, small shoulders at ∼2870, ∼2848, ∼1620, and ∼1552 cm^{-1} also develop in the spectra. This complex spectrum evolves with time with bands at 2866, 2854, 1612, 1583, and 1560 cm^{-1} dominating after 210 min of irradiation (Figure 4, lower panels). Note that the spectrum exhibits additional bands at 1380, 1360, and 1327 cm^{-1}, which also develop upon extended exposure to visible light. The existence of isosbestic points in the C−H stretching region (Figure 4C) indicates direct conversion of methoxy groups (the negative bands at 2910 and 2811 cm^{-1}) into formate products (the broad positive band at 2866 cm^{-1} with shoulder at 2854 cm^{-1}).[59,137,138] The small bands at 2956 and 2744 cm^{-1} are attributed to [ν_{as}(OCO) + δ(CH)] and two δ(CH) modes, respectively.[138,139] In the low wavenumber region (Figure 4D), the methoxy depletion is highlighted by negative bands below 1200 cm^{-1}, while the production of formates is indicated by the positive bands in this region of the spectrum.[59,137,138] The spectral development observed in an analogous experiment, but under UV irradiation, is presented in Figure S8A, B, Supporting Information.

Our results demonstrate that the Au−TiO_2 photoactive system leads to identical products under both UV- and visible-light irradiation, most likely driven by a direct hole-attachment mechanism involving multielectron oxidation. Clearly, the photophysical origin of the charge carriers differs for these two irradiation regimes. Under UV irradiation, electron−hole-pair generation occurs directly upon absorption of supra-band

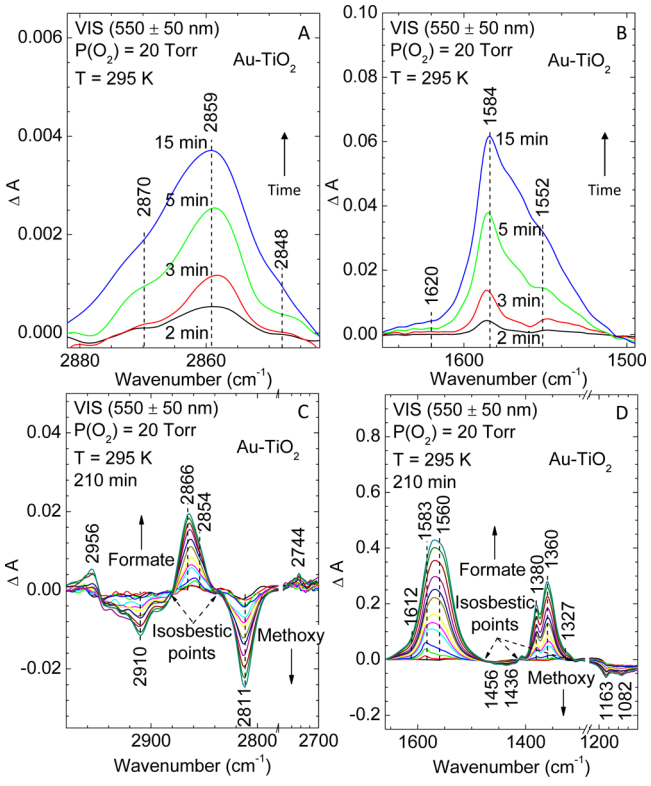

Figure 4. Time-resolved development of IR modes during visible-light-induced methoxy-to-formate conversion on Au−TiO_2 aerogel under aerobic conditions: (A, B) the initial 15 min of reaction time; (C, D) reaction time extended to 210 min.

gap energy photons, while local surface plasmon resonances drive the generation of electrons during visible-light irradiation. Under both irradiation regimes, oxygen likely behaves as a scavenger of excess electrons, which depletes surface charge enabling the diffusion of holes to the surface. The role of surface O_2 as an electron scavenger (as opposed to a reactant) is supported by the fact that the chemistry does not proceed beyond the creation of surface-bound formates. Even though highly aggressive oxidative catalysis has been shown to fully combust surface-adsorbed organics to CO_2 through the activation and addition of molecular oxygen, we observe only trace amounts of CO_2, even in the presence of a constant 20 Torr background pressure of oxygen.

3.5.3. Formate Bonding Structure and Band Assignments. Different bonding configurations have been proposed in previous experimental and theoretical studies into the structure and vibrational spectrum of formates, including a relatively unstable chelating bidentate structure, a monodentate geometry, and bridging bidentate configuration.[140−144] Boccuzzi et al., in studying the thermal decomposition of methanol on Au/TiO_2 nanoparticles, observed bands at 2864, 1567, 1380, and 1359 cm^{-1} that were attributed to bidentate formate species bound to single Ti sites.[59] Additional bands that appeared at 2950, 1632, and 1312 cm^{-1} in their work were assigned to formate species bound in a bidentate configuration to a single Au site.[59] However, no IR bands attributable to formates bound to Au sites were found during recent studies of the water−gas shift reaction over Au/CeO_2 nanoparticles.[145] Instead, the existence of formates bound to Ce^{3+} (bands at 2848, 1585, and 1370 cm^{-1}) and Ce^{4+} (bands at 2949, 1550, and 1370 cm^{-1}) were reported.

On the basis of previous work and the analysis of the spectral data in Figure 4, we hypothesize that surface formates created during irradiation of Au−TiO_2 aerogel are bound to three distinct surface sites. The set of bands at 2859 cm^{-1} (C−H stretch), 1584 cm^{-1} [ν_{as}(OCO)], and 1360 cm^{-1} [ν_s(OCO)] most likely arises from formates bound to low coordinated titanium atoms that border the titania support and Au nanoparticles. This assignment is based on the observation that the band at 1584 cm^{-1} is missing from the spectrum of UV-irradiated TiO_2 aerogel, which exhibits high levels of surface-bound formates (Figure S8D, Supporting Information; see also the deconvolution of bands shown in Figure S9, Supporting Information). On the basis of the measured ν_{as}(COO)−ν_s(COO) splitting ($\Delta\nu_{as-s}$) of 224 cm^{-1}, these modes likely belong to a different class of formates that reside on the surface as a bidentate bridge-bound species.[140] The assignment of bidentate bridge-bound formates is further supported by the emergence of a set of bands at 2866 cm^{-1} (C−H stretch), 1560 cm^{-1} [ν_{as}(OCO)], and 1360 cm^{-1} [ν_s(OCO)] that appear for visible-light-irradiated Au−TiO_2 and UV-exposed TiO_2 aerogel, which suggests that these formates are bound to Ti sites on the titania support.[59,60,137] A third type of surface-associated formate that may be present following methanol oxidation is evidenced by the set of bands at 2854 cm^{-1} (C−H stretch), 1612 cm^{-1} [ν_{as}(OCO)], and 1327 cm^{-1} [ν_s(OCO)]. The species associated with these IR modes are likely monodentate ester-type formates ($\Delta\nu_{as-s}$ = 285 cm^{-1}) bound to on-top Ti sites. An analogous set of bands observed during thermal decomposition of methanol were assigned as formates bound to on-top Au sites.[59,137] Because we observe the same bands for TiO_2 aerogel (Figure S8, Supporting Information), these modes are not due to interactions with Au atoms. Therefore, we tentatively assign these bands to the monodentate formate bonded to on-top titanium sites.

4. SUMMARY

Our initial investigation of the photochemistry of methanol adsorbed at networked TiO_2 and Au−TiO_2 aerogels reveals both some anticipated and some exceptional chemical and photochemical properties of the 3D Au−TiO_2 nanoarchitecture. Under dark, high-vacuum conditions, methanol dissociatively adsorbs at the surfaces of 3D TiO_2 and Au−TiO_2 aerogels. As expected for TiO_2-based materials, CH_3OH binds to coordinatively unsaturated Ti sites at TiO_2 and Au−TiO_2 aerogels, forming stable bound methoxy species and protonating the TiO_2 surface to form stable surface hydroxyls. On the Au−TiO_2 aerogels, an additional binding mode is possible under dark conditions, because highly reactive Au−O−Ti linkages oxidize methanol to produce adsorbed carboxylate species.

Upon irradiation of both materials with broadband UV light under anaerobic conditions, adsorbed methoxy groups act as hole-trapping centers, extending the lifetime of conduction-band electrons and shallow-trapped electrons. These long-lived excited states are observable as an increase in the background IR absorption spectrum (1000−4000 cm^{-1}) of both materials, with a broad maximum centered between 1100 and 1700 cm^{-1}. Additionally, expressing TiO_2 as an aerogel yields a form of nanoscale TiO_2 that more efficiently generates long-lived electron−hole pairs under UV irradiation than does a commercial P25 sample of TiO_2. This observation is consistent with other recent reports of efficient charge separation in

dx.doi.org/10.1021/jp312583w | J. Phys. Chem. C 2013, 117, 15035−15049

nanoscale networks[28,114,115] and further demonstrates the enabling role that well-connected nanoscale pathways play in the transport of charge within functional materials.

Upon excitation with narrow-band visible light centered at 550 nm, long-lived excited-state electrons are evident on CH_3OH-exposed Au−TiO_2 aerogels, but not on identically treated TiO_2 aerogels, indicating that incorporated Au nanoparticles sensitize the TiO_2 aerogel network to visible light. Admission of O_2 to the reactor quenches the broad background IR absorbance of irradiated, CH_3OH-exposed TiO_2 and Au−TiO_2 aerogels, because O_2 scavenges the photogenerated conduction-band and shallow-trapped electrons from the semiconductor.

Under aerobic reaction conditions and broadband-UV illumination, accumulation of surface formates via oxidation of adsorbed methoxy species occurs at similar rates on Au−TiO_2 and TiO_2 aerogels. When exposed to narrow-band visible excitation centered at 550 nm, Au−TiO_2 photochemically converts surface-bound methoxy groups to formates at rates comparable to their production on TiO_2 aerogels under broadband UV illumination, whereas no photochemical oxidation activity is observed on TiO_2 aerogels under irradiation at wavelengths longer than 400 nm. The magnitude of visible-light-driven oxidative activity at Au−TiO_2 aerogels tracks the shape of the SPR spectrum of the incorporated Au nanoparticles. Both the fast photochemical oxidation rates under illumination at the SPR maximum of Au−TiO_2 aerogels and the qualitative coincidence between the wavelength-dependence of photocatalytic activity and the SPR feature indicate a strong sensitizing role of the incorporated Au nanoparticles.

The visible-light-driven photochemical oxidation activity, high stability, and high surface area of 3D Au−TiO_2 make it an appealing candidate for applications such as visible-light-driven photochemical degradation of environmental pollutants. More broadly, the networked, three-dimensional nanoscale design and the available dynamic range of incorporated Au content[38,146] make 3D Au−TiO_2 a flexible model system for future work aimed at determining the complex interplay between the roles of incorporated plasmonic metal nanoparticles as (i) visible-light sensitizers, (ii) a means to increase electron−hole lifetimes by localizing electrons, and (conversely) (iii) recombination centers that *decrease* electron−hole lifetime in 3D-nanostructured photoactive materials.

■ ASSOCIATED CONTENT

Supporting Information

Schematic representation of the catalyst, characterization of the aerogel by TEM, XRD, and diffuse reflectance, and IR spectra of aerogels. This information is available free of charge via the Internet athttp://pubs.acs.org.

■ AUTHOR INFORMATION

Corresponding Author

*J.R.M.: telephone (540) 231-2472; E-mail jrmorris@vt.edu. J.J.P.: telephone (202) 767-8135; e-mail: jeremy.pietron@nrl.navy.mil.

Notes

The authors declare no competing financial interest.

■ ACKNOWLEDGMENTS

The authors wish to thank Dr. Charles Bass for initiating this fruitful collaboration. J.R.M. thanks Mr. Fred Blair for many hours of instrument making. This work was supported through Grants from the Army Research Office (W911NF-09-1-0150), the Defense Threat Reduction Agency (W911NF-06-1-0111), and the Office of Naval Research. In addition, helpful insight, advice, and use of instrumentation were provided by Dr. Brian Tissue. The authors would also like to thank Dr. Jeffrey Owrutsky (NRL) and the members of Code 6171 (NRL) for helpful discussions of the results of the present study. P. A. DeSario is an NRC Postdoctoral Associate, and Lindsey C. Szymczak is a STEP Research Aide in Code 6170.

■ REFERENCES

(1) Thompson, T. L.; Yates, J. T., Jr. Surface Science Studies of the Photoactivation of TiO_2−New Photochemical Processes. *Chem. Rev.* **2006**, *106* (10), 4428−4453.

(2) Linsebigler, A. L.; Lu, G. Q.; Yates, J. T., Jr. Photocatalysis on TiO_2 Surfaces−Principles, Mechanisms, and Selected Results. *Chem. Rev.* **1995**, *95* (3), 735−758.

(3) Hoffmann, M. R.; Martin, S. T.; Choi, W. Y.; Bahnemann, D. W. Environmental Applications of Semiconductor Photocatalysis. *Chem. Rev.* **1995**, *95* (1), 69−96.

(4) Palmisano, G.; Augugliaro, V.; Pagliaro, M.; Palmisano, L. Photocatalysis: A Promising Route for 21st Century Organic Chemistry. *Chem. Commun.* **2007**, *33*, 3425−3437.

(5) Ohtani, B. Preparing Articles on Photocatalysis−Beyond the Illusions, Misconceptions, and Speculation. *Chem. Lett.* **2008**, *37* (3), 216−229.

(6) Primo, A.; Corma, A.; Garcia, H. Titania Supported Gold Nanoparticles as Photocatalyst. *Phys. Chem. Chem. Phys.* **2011**, *13* (3), 886−910.

(7) Henderson, M. A. A Surface Science Perspective on Photocatalysis. *Surf. Sci. Rep.* **2011**, *66* (6−7), 185−297.

(8) Górska, P.; Zaleska, A.; Kowalska, E.; Klimczuk, T.; Sobczak, J. W.; Skwarek, E.; Janusz, W.; Hupka, J. TiO_2 Photoactivity in Vis and UV Light: The Influence of Calcination Temperature and Surface Properties. *Appl. Catal., B* **2008**, *84* (3−4), 440−447.

(9) Chen, X.; Shen, S.; Guo, L.; Mao, S. S. Semiconductor-Based Photocatalytic Hydrogen Generation. *Chem. Rev.* **2010**, *110* (11), 6503−6570.

(10) Kamat, P. V. Photophysical, Photochemical and Photocatalytic Aspects of Metal Nanoparticles. *J. Phys. Chem. B* **2002**, *106* (32), 7729−7744.

(11) Tian, Y.; Tatsuma, T. Mechanisms and Applications of Plasmon-Induced Charge Separation at TiO_2 Films Loaded with Gold Nanoparticles. *J. Am. Chem. Soc.* **2005**, *127* (20), 7632−7637.

(12) Hartland, G. V. Optical Studies of Dynamics in Noble Metal Nanostructures. *Chem. Rev.* **2011**, *111* (6), 3858−3887.

(13) Furube, A.; Du, L.; Hara, K.; Katoh, R.; Tachiya, M. Ultrafast Plasmon-Induced Electron Transfer from Gold Nanodots into TiO_2 Nanoparticles. *J. Am. Chem. Soc.* **2007**, *129* (48), 14852−14853.

(14) Du, L.; Furube, A.; Yamamoto, K.; Hara, K.; Katoh, R.; Tachiya, M. Plasmon-Induced Charge Separation and Recombination Dynamics in Gold−TiO_2 Nanoparticle Systems: Dependence on TiO_2 Particle Size. *J. Phys. Chem. C* **2009**, *113* (16), 6454−6462.

(15) Kowalska, E.; Abe, R.; Ohtani, B. Visible Light-Induced Photocatalytic Reaction of Gold-Modified Titanium(IV) Oxide Particles: Action Spectrum Analysis. *Chem. Commun.* **2009**, *2*, 241−243.

(16) Linic, S.; Christopher, P.; Ingram, D. B. Plasmonic-Metal Nanostructures for Efficient Conversion of Solar to Chemical Energy. *Nat. Mater.* **2011**, *10* (12), 911−921.

(17) Kowalska, E.; Mahaney, O. O. P.; Abe, R.; Ohtani, B. Visible-Light-Induced Photocatalysis through Surface Plasmon Excitation of

Gold on Titania Surfaces. *Phys. Chem. Chem. Phys.* **2010**, *12* (10), 2344−2355.
(18) Mayer, K. M.; Hafner, J. H. Localized Surface Plasmon Resonance Sensors. *Chem. Rev.* **2011**, *111* (6), 3828−3857.
(19) Kimura, K.; Naya, S.-i.; Jin-nouchi, Y.; Tada, H. TiO_2 Crystal Form-Dependence of the Au/TiO_2 Plasmon Photocatalyst's Activity. *J. Phys. Chem. C* **2012**, *116* (12), 7111−7117.
(20) Myroshnychenko, V.; Rodriguez-Fernandez, J.; Pastoriza-Santos, I.; Funston, A. M.; Novo, C.; Mulvaney, P.; Liz-Marzan, L. M.; Garcia de Abajo, F. J. Modelling the Optical Response of Gold Nanoparticles. *Chem. Soc. Rev.* **2008**, *37* (9), 1792−1805.
(21) Zhang, Z.; Yates, J. T. Band Bending in Semiconductors: Chemical and Physical Consequences at Surfaces and Interfaces. *Chem. Rev.* **2012**, *112*, 5520−5551.
(22) Garcia, M. A. Surface Plasmons in Metallic Nanoparticles: Fundamentals and Applications. *J. Phys. D: Appl. Phys.* **2011**, *44* (28), No. 283001.
(23) Du, L.; Furube, A.; Hara, K.; Katoh, R.; Tachiya, M. Ultrafast Plasmon Induced Electron Injection Mechanism in Gold−TiO_2 Nanoparticle System. *J. Photochem. Photobiol., C* **2013**, *15*, 21−30.
(24) Zhang, Q.; Lima, D. Q.; Lee, I.; Zaera, F.; Chi, M.; Yin, Y. A Highly Active Titanium Dioxide Based Visible-Light Photocatalyst with Nonmetal Doping and Plasmonic Metal Decoration. *Angew. Chem., Int. Ed.* **2011**, *50* (31), 7088−7092.
(25) Gomes Silva, C.; Juárez, R.; Marino, T.; Molinari, R.; García, H. Influence of Excitation Wavelength (UV or Visible Light) on the Photocatalytic Activity of Titania Containing Gold Nanoparticles for the Generation of Hydrogen or Oxygen from Water. *J. Am. Chem. Soc.* **2010**, *133* (3), 595−602.
(26) Ismail, A. A.; Bahnemann, D. W.; Bannat, I.; Wark, M. Gold Nanoparticles on Mesoporous Interparticle Networks of Titanium Dioxide Nanocrystals for Enhanced Photonic Efficiencies. *J. Phys. Chem. C* **2009**, *113* (17), 7429−7435.
(27) Heiligtag, F. J.; Rossell, M. D.; Suess, M. J.; Niederberger, M. Template-Free Co-Assembly of Preformed Au and TiO_2 Nanoparticles into Multicomponent 3D Aerogels. *J. Mater. Chem.* **2011**, *21* (42), 16893−16899.
(28) Peter, A.; Baia, L.; Baia, M.; Indrea, E.; Toderas, F.; Danciu, V.; Cosoveanu, V.; Diamandescu, L. Porous Au-TiO_2 Aerogels Nanoarchitectures for Photodegradation Processes. *J. Optoelectron. Adv. Mater.* **2010**, *12*, 1071−1077.
(29) Bannat, I.; Wessels, K.; Oekermann, T.; Rathousky, J.; Bahnemann, D.; Wark, M. Improving the Photocatalytic Performance of Mesoporous Titania Films by Modification with Gold Nanostructures. *Chem. Mater.* **2009**, *21* (8), 1645−1653.
(30) Zhao, J.; Sallard, S.; Smarsly, B. M.; Gross, S.; Bertino, M.; Boissiere, C.; Chen, H.; Shi, J. Photocatalytic Performances of Mesoporous TiO_2 Films Doped with Gold Clusters. *J. Mater. Chem.* **2010**, *20* (14), 2831−2839.
(31) Wang, X.; Mitchell, D. R. G.; Prince, K.; Atanacio, A. J.; Caruso, R. A. Gold Nanoparticle Incorporation into Porous Titania Networks Using an Agarose Gel Templating Technique for Photocatalytic Applications. *Chem. Mater.* **2008**, *20* (12), 3917−3926.
(32) Neatu, S.; Cojocaru, B.; Parvulescu, V. I.; Somoghi, V.; Alvaro, M.; Garcia, H. Visible-Light C-Heteroatom Bond Cleavage and Detoxification of Chemical Warfare Agents Using Titania-Supported Gold Nanoparticles as Photocatalyst. *J. Mater. Chem.* **2010**, *20* (20), 4050−4054.
(33) Hüsing, N.; Schubert, U. Aerogels—Airy Materials: Chemistry, Structure, and Properties. *Angew. Chem., Int. Ed.* **1998**, *37* (1−2), 22−45.
(34) Pierre, A. C.; Pajonk, G. M. Chemistry of Aerogels and Their Applications. *Chem. Rev.* **2002**, *102* (11), 4243−4266.
(35) Long, J. W.; Rolison, D. R. Architectural Design, Interior Decoration, and Three-Dimensional Plumbing En Route to Multifunctional Nanoarchitectures. *Acc. Chem. Res.* **2007**, *40* (9), 854−862.
(36) Morris, C. A.; Anderson, M. L.; Stroud, R. M.; Merzbacher, C. I.; Rolison, D. R. Silica Sol as a Nanoglue: Flexible Synthesis of Composite Aerogels. *Science* **1999**, *284* (5414), 622−624.
(37) Anderson, M. L.; Morris, C. A.; Stroud, R. M.; Merzbacher, C. I.; Rolison, D. R. Colloidal Gold Aerogels: Preparation, Properties, and Characterization. *Langmuir* **1999**, *15* (3), 674−681.
(38) Pietron, J. J.; Stroud, R. M.; Rolison, D. R. Using Three Dimensions in Catalytic Mesoporous Nanoarchitectures. *Nano Lett.* **2002**, *2* (5), 545−549.
(39) Shen, M.; Henderson, M. A. Identification of the Active Species in Photochemical Hole Scavenging Reactions of Methanol on TiO_2. *J. Phys. Chem. Lett.* **2011**, *2* (21), 2707−2710.
(40) Shen, M.; Henderson, M. A. Role of Water in Methanol Photochemistry on Rutile TiO_2(110). *J. Phys. Chem. C* **2012**, *116* (35), 18788−18795.
(41) Yuan, Q.; Wu, Z.; Jin, Y.; Xu, L.; Xiong, F.; Ma, Y.; Huang, W. Photocatalytic Cross-Coupling of Methanol and Formaldehyde on a Rutile TiO_2(110) Surface. *J. Am. Chem. Soc.* **2013**, *135* (13), 5212−5219.
(42) Panayotov, D. A.; Burrows, S. P.; Yates, J. T.; Morris, J. R. Mechanistic Studies of Hydrogen Dissociation and Spillover on Au/TiO_2: IR Spectroscopy of Coadsorbed CO and H-Donated Electrons. *J. Phys. Chem. C* **2011**, *115* (45), 22400−22408.
(43) Kim, W.-I.; Suh, D.; Park, T.-J.; Hong, I.-K. Photocatalytic Degradation of Methanol on Titania and Titania−Silica Aerogels Prepared by Non-Alkoxide Sol−Gel Route. *Top. Catal.* **2007**, *44* (4), 499−505.
(44) Brust, M.; Walker, M.; Bethell, D.; Schiffrin, D. J.; Whyman, R. Synthesis of Thiol-Derivatised Gold Nanoparticles in a Two-Phase Liquid-Liquid System. *J. Chem. Soc., Chem. Commun.* **1994**, *7*, 801−802.
(45) Hostetler, M. J.; Templeton, A. C.; Murray, R. W. Dynamics of Place-Exchange Reactions on Monolayer-Protected Gold Cluster Molecules. *Langmuir* **1999**, *15* (11), 3782−3789.
(46) Templeton, A. C.; Wuelfing, W. P.; Murray, R. W. Monolayer-Protected Cluster Molecules. *Acc. Chem. Res.* **1999**, *33* (1), 27−36.
(47) Hostetler, M. J.; Green, S. J.; Stokes, J. J.; Murray, R. W. Monolayers in Three Dimensions: Synthesis and Electrochemistry of Ω-Functionalized Alkanethiolate-Stabilized Gold Cluster Compounds. *J. Am. Chem. Soc.* **1996**, *118* (17), 4212−4213.
(48) Dagan, G.; Tomkiewicz, M. Titanium Dioxide Aerogels for Photocatalytic Decontamination of Aquatic Environments. *J. Phys. Chem.* **1993**, *97* (49), 12651−12655.
(49) Harkins, W. D.; Jura, G. Surfaces of Solids. XII. An Absolute Method for the Determination of the Area of a Finely Divided Crystalline Solid. *J. Am. Chem. Soc.* **1944**, *66* (8), 1362−1366.
(50) Highly Dispersed Metallic Oxides Produced by Aerosil Process. *Highly Dispersed Metallic Oxides Produced by Aerosil Process. Degussa Technical Bulletin Pigments*; Degussa AG: Frankfurt, Germany, 1990; Vol. 56, p 13.
(51) Addamo, M.; Augugliaro, V.; Di Paola, A.; Garcia-Lopez, E.; Loddo, V.; Marci, G.; Molinari, R.; Palmisano, L.; Schiavello, M. Preparation, Characterization, and Photoactivity of Polycrystalline Nanostructured TiO_2 Catalysts. *J. Phys. Chem. B* **2004**, *108* (10), 3303−3310.
(52) Mawhinney, D. B.; Rossin, J. A.; Gerhart, K.; Yates, J. T. Adsorption Studies by Transmission IR Spectroscopy: A New Method for Opaque Materials. *Langmuir* **1999**, *15* (13), 4617−4621.
(53) Thompson, T. L.; Panayotov, D. A.; Yates, J. T., Jr. Adsorption and Thermal Decomposition of 2-Chloroethyl Ethyl Sulfide on TiO_2 Surfaces. *J. Phys. Chem. B* **2004**, *108*, 16825−16833.
(54) Panayotov, D. A.; Burrows, S. P.; Morris, J. R. Infrared Spectroscopic Studies of Conduction Band and Trapped Electrons in UV-Photoexcited, H-Atom N-Doped, and Thermally Reduced TiO_2. *J. Phys. Chem. C* **2012**, *116* (7), 4535−4544.
(55) Panayotov, D. A.; Morris, J. R. Thermal Decomposition of a Chemical Warfare Agent Simulant (DMMP) on TiO_2: Adsorbate Reactions with Lattice Oxygen as Studied by Infrared Spectroscopy. *J. Phys. Chem. C* **2009**, *113* (35), 15684−15691.
(56) Panayotov, D. A.; Morris, J. R. Catalytic Degradation of a Chemical Warfare Agent Simulant: Reaction Mechanisms on TiO_2-Supported Au Nanoparticles. *J. Phys. Chem. C* **2008**, *112*, 7496−7502.

(57) Panayotov, D. A.; Burrows, S.; Mihaylov, M.; Hadjiivanov, K.; Tissue, B. M.; Morris, J. R. Effect of Methanol on the Lewis Acidity of Rutile TiO_2 Nanoparticles Probed through Vibrational Spectroscopy of Coadsorbed CO. *Langmuir* **2010**, *26* (11), 8106−8112.
(58) Panayotov, D. A.; Burrows, S. P.; Morris, J. R. Photooxidation Mechanism of Methanol on Rutile TiO_2 Nanoparticles. *J. Phys. Chem. C* **2012**, *116* (11), 6623−6635.
(59) Boccuzzi, F.; Chiorino, A.; Manzoli, M. FTIR Study of Methanol Decomposition on Gold Catalyst for Fuel Cells. *J. Power Sources* **2003**, *118* (1−2), 304−310.
(60) Nuhu, A.; Soares, J.; Gonzalez-Herrera, M.; Watts, A.; Hussein, G.; Bowker, M. Methanol Oxidation on Au/TiO_2 Catalysts. *Top. Catal.* **2007**, *44* (1), 293−297.
(61) Hadjiivanov, K. I.; Klissurski, D. G. Surface Chemistry of Titania (Anatase) and Titania Supported Catalysts. *Chem. Soc. Rev.* **1996**, *25* (1), 61.
(62) Hussein, G. A. M.; Sheppard, N.; Zaki, M. I.; Fahim, R. B. Infrared Spectroscopic Studies of the Reactions of Alcohols over Group IVB Metal Oxide Catalysts. Part 2. Methanol over TiO_2, ZrO, and HfO_2. *J. Chem. Soc., Faraday Trans.* **1991**, *87*, 2655−2659.
(63) Wang, C.-y.; Groenzin, H.; Shultz, M. J. Surface Characterization of Nanoscale TiO_2 Film by Sum Frequency Generation Using Methanol as a Molecular Probe. *J. Phys. Chem. B* **2003**, *108* (1), 265−272.
(64) Wang, C.-y.; Groenzin, H.; Shultz, M. J. Direct Observation of Competitive Adsorption between Methanol and Water on TiO_2: An in Situ Sum-Frequency Generation Study. *J. Am. Chem. Soc.* **2004**, *126* (26), 8094−8095.
(65) Suda, Y.; Morimoto, T.; Nagao, M. Adsorption of Alcohols on Titanium Dioxide (Rutile) Surface. *Langmuir* **1987**, *3*, 99−104.
(66) Taylor, E. A.; Griffin, G. L. Product Selectivity during CH_3OH Decomposition on TiO_2 Powders. *J. Phys. Chem.* **1988**, *92*, 477−481.
(67) Wu, W.-C.; Chuang, C.-C.; Lin, J.-L. Bonding Geometry and Reactivity of Methoxy and Ethoxy Groups Adsorbed on Powdered TiO_2. *J. Phys. Chem. B* **2000**, *104* (36), 8719−8724.
(68) Bronkema, J. L.; Leo, D. C.; Bell, A. T. Mechanistic Studies of Methanol Oxidation to Formaldehyde on Isolated Vanadate Sites Supported on High Surface Area Anatase. *J. Phys. Chem. C* **2007**, *111* (39), 14530−14540.
(69) Chabal, Y. J. Surface Infrared Spectroscopy. *Surf. Sci. Rep.* **1988**, *8* (5−7), 211−357.
(70) Badri, A.; Binet, C.; Lavalley, J.-C. Use of Methanol as an IR Molecular Probe to Study the Surface of Polycrystalline Ceria. *J. Chem. Soc., Faraday Trans.* **1997**, *93*, 1159−1168.
(71) Hadjiivanov, K. I.; Vayssilov, G. N. Characterization of Oxide Surfaces and Zeolites by Carbon Monoxide as an IR Probe Molecule. *Adv. Catal.* **2002**, *47*, 307−511.
(72) Meyer, R.; Lemire, C.; Shaikhutdinov, S. K.; Freund, H.-J. Surface Chemistry of Catalysis by Gold. *Gold Bull.* **2004**, *37*, 72.
(73) Rupprechter, G. 8 Surface Vibrational Spectroscopy on Noble Metal Catalysts from Ultrahigh Vacuum to Atmospheric Pressure. *Annu. Rep. Prog. Chem., Sect. C: Phys. Chem.* **2004**, *100*, 237−311.
(74) Fierro-Gonzalez, J. C.; Gates, B. C. Evidence of Active Species in CO Oxidation Catalyzed by Highly Dispersed Supported Gold. *Catal. Today* **2007**, *122* (3−4), 201−210.
(75) Zaki, M. I.; Knözinger, H. An Infrared Spectroscopy Study of Carbon Monoxide Adsorption on [Alpha]-Chromia Surfaces: Probing Oxidation States of Coordinatively Unsaturated Surface Cations. *J. Catal.* **1989**, *119* (2), 311−321.
(76) Bond, G. C.; Thompson, D. T. Gold-Catalysed Oxidation of Carbon Monoxide. *Gold Bull.* **2000**, *33*, 41−50.
(77) Liu, L.; Zhou, Z.; Guo, Q.; Yan, Z.; Yao, Y.; Goodman, D. W. The 2-D Growth of Gold on Single-Layer Graphene/Ru(0001): Enhancement of CO Adsorption. *Surf. Sci.* **2011**, *605* (17−18), L47−L50.
(78) Bagus, P. S.; Pacchioni, G. On the Origin of Bonding and Vibrational Frequency Shifts for CO Adsorbed on Neutral, Cationic and Anionic Gold Clusters. *J. Phys.: Conf. Ser.* **2008**, *117*, No. 012003.
(79) Meier, D. C.; Goodman, D. W. The Influence of Metal Cluster Size on Adsorption Energies: CO Adsorbed on Au Clusters Supported on TiO_2. *J. Am. Chem. Soc.* **2004**, *126* (6), 1892−1899.
(80) Fohlisch, A.; Nyberg, M.; Bennich, P.; Triguero, L.; Hasselstrom, J.; Karis, O.; Pettersson, L. G. M.; Nilsson, A. The Bonding of CO to Metal Surfaces. *J. Chem. Phys.* **2000**, *112* (4), 1946−1958.
(81) Morterra, C. An Infrared Spectroscopic Study of Anatase Properties. Part 6.-Surface Hydration and Strong Lewis Acidity of Pure and Sulphate-Doped Preparations. *J. Chem. Soc., Faraday Trans. 1* **1988**, *84*, 1617−1637.
(82) Busca, G.; Saussey, H.; Saur, O.; Lavalley, J. C.; Lorenzelli, V. FT-IR Characterization of the Surface Acidity of Different Titanium Dioxide Anatase Preparations. *Appl. Catal.* **1985**, *14*, 245−260.
(83) Hadjiivanov, K.; Lamotte, J.; Lavalley, J.-C. FTIR Study of Low-Temperature CO Adsorption on Pure and Ammonia-Precovered TiO_2 (Anatase). *Langmuir* **1997**, *13* (13), 3374−3381.
(84) Martra, G. Lewis Acid and Base Sites at the Surface of Microcrystalline TiO_2 Anatase: Relationships between Surface Morphology and Chemical Behaviour. *Appl. Catal., A* **2000**, *200* (1−2), 275−285.
(85) Boccuzzi, F.; Chiorino, A.; Tsubota, S.; Haruta, M. FTIR Study of Carbon Monoxide Oxidation and Scrambling at Room Temperature over Gold Supported on ZnO and TiO_2. *J. Phys. Chem.* **1996**, *100* (9), 3625−3631.
(86) Grunwaldt, J.-D.; Maciejewski, M.; Becker, O. S.; Fabrizioli, P.; Baiker, A. Comparative Study of Au/TiO_2 and Au/ZrO_2 Catalysts for Low-Temperature CO Oxidation. *J. Catal.* **1999**, *186* (2), 458−469.
(87) Venkov, T.; Fajerwerg, K.; Delannoy, L.; Klimev, H.; Hadjiivanov, K.; Louis, C. Effect of the Activation Temperature on the State of Gold Supported on Titania: An FT-IR Spectroscopic Study. *Appl. Catal., A* **2006**, *301* (1), 106−114.
(88) Klimev, H.; Fajerwerg, K.; Chakarova, K.; Delannoy, L.; Louis, C.; Hadjiivanov, K. Oxidation of Gold Metal Particles Supported on TiO_2: An FTIR Study by Means of Low-Temperature CO Adsorption. *J. Mater. Sci.* **2007**, *42* (10), 3299−3306.
(89) Green, I. X.; Tang, W.; Neurock, M.; Yates, J. T. Spectroscopic Observation of Dual Catalytic Sites During Oxidation of CO on a Au/TiO_2 Catalyst. *Science* **2011**, *333* (6043), 736−739.
(90) Mavrikakis, M.; Stoltze, P.; Nørskov, J. K. Making Gold Less Noble. *Catal. Lett.* **2000**, *64*, 101.
(91) Wang, J.; Hammer, B. Oxidation State of Oxide Supported Nanometric Gold. *Top. Catal.* **2007**, *44* (1), 49−56.
(92) Bond, G.; Thompson, D. Catalysis by Gold. *Catal. Rev. Sci. Eng.* **1999**, *41* (3/4), 319.
(93) Boccuzzi, F.; Chiorino, A.; Manzoli, M. FTIR Study of the Electronic Effects of CO Adsorbed on Gold Nanoparticles Supported on Titania. *Surf. Sci.* **2000**, *454−456*, 942−946.
(94) Maciejewski, M.; Fabrizioli, P.; Grunwaldt, J.-D.; Becker, O. S.; Baiker, A. Supported Gold Catalysts for CO Oxidation: Effect of Calcination on Structure, Adsorption and Catalytic Behaviour. *Phys. Chem. Chem. Phys.* **2001**, *3* (17), 3846−3855.
(95) Manzoli, M.; Chiorino, A.; Boccuzzi, F. FTIR Study of Nanosized Gold on ZrO_2 and TiO_2. *Surf. Sci.* **2003**, *532−535*, 377−382.
(96) Boronat, M.; Concepción, P.; Corma, A. Unravelling the Nature of Gold Surface Sites by Combining IR Spectroscopy and DFT Calculations. Implications in Catalysis. *J. Phys. Chem. C* **2009**, *113* (38), 16772−16784.
(97) Vindigni, F.; Manzoli, M.; Chiorino, A.; Boccuzzi, F. Catalytically Active Gold Sites: Nanoparticles, Borderline Sites, Clusters, Cations, Anions? FTIR Spectra Analysis of ^{12}CO and of ^{12}CO-^{13}CO Isotopic Mixtures. *Gold Bull.* **2009**, *42* (2), 106.
(98) Davydov, A. A.; Shepot'ko, M. L. Forms of Adsorption of Methanol on Anatase and Directions of Their Transformation. *Theor. Exp. Chem.* **1988**, *24* (6), 676−681.
(99) Gong, X.-Q.; Selloni, A. Reactivity of Anatase TiO_2 Nanoparticles: The Role of the Minority (001) Surface. *J. Phys. Chem. B* **2005**, *109* (42), 19560−19562.

(100) Sorescu, D. C.; Yates, J. T. Adsorption of CO on the TiO_2(110) Surface: A Theoretical Study. *J. Phys. Chem. B* **1998**, *102* (23), 4556−4565.
(101) Han, Y.; Liu, C.-j.; Ge, Q. Effect of Pt Clusters on Methanol Adsorption and Dissociation over Perfect and Defective Anatase TiO_2(101) Surface. *J. Phys. Chem. C* **2009**, *113* (48), 20674−20682.
(102) Bates, S. P.; Gillan, M. J.; Kresse, G. Adsorption of Methanol on TiO_2(110): A First-Principles Investigation. *J. Phys. Chem. B* **1998**, *102* (11), 2017−2026.
(103) Tilocca, A.; Selloni, A. Methanol Adsorption and Reactivity on Clean and Hydroxylated Anatase(101) Surfaces. *J. Phys. Chem. B* **2004**, *108* (50), 19314−19319.
(104) Ahmed, A. Y.; Kandiel, T. A.; Oekermann, T.; Bahnemann, D. Photocatalytic Activities of Different Well-Defined Single Crystal TiO_2 Surfaces: Anatase Versus Rutile. *J. Phys. Chem. Lett.* **2011**, *2* (19), 2461−2465.
(105) Yamakata, A.; Ishibashi, T.-a.; Onishi, H. Time-Resolved Infrared Absorption Spectroscopy of Photogenerated Electrons in Platinized TiO_2 Particles. *Chem. Phys. Lett.* **2001**, *333* (3−4), 271−277.
(106) Szczepankiewicz, S. H.; Moss, J. A.; Hoffmann, M. R. Slow Surface Charge Trapping Kinetics on Irradiated TiO_2. *J. Phys. Chem. B* **2002**, *106* (11), 2922−2927.
(107) Berger, T.; Sterrer, M.; Diwald, O.; Knözinger, E.; Panayotov, D.; Thompson, T. L.; Yates, J. T., Jr. Light-Induced Charge Separation in Anatase TiO_2 Particles. *J. Phys. Chem. B* **2005**, *109* (13), 6061−6068.
(108) Fujishima, A.; Zhang, X.; Tryk, D. A. TiO_2 Photocatalysis and Related Surface Phenomena. *Surf. Sci. Rep.* **2008**, *63* (12), 515−582.
(109) Ghosh, A. K.; Wakim, F. G.; Addiss, R. R. Photoelectronic Processes in Rutile. *Phys. Rev.* **1969**, *184* (3), 979.
(110) Thompson, T. L.; Yates, J. T., Jr. Monitoring Hole Trapping in Photoexcited TiO_2(110) Using a Surface Photoreaction. *J. Phys. Chem. B* **2005**, *109* (39), 18230−18236.
(111) Tamaki, Y.; Furube, A.; Murai, M.; Hara, K.; Katoh, R.; Tachiya, M. Direct Observation of Reactive Trapped Holes in TiO_2 Undergoing Photocatalytic Oxidation of Adsorbed Alcohols: Evaluation of the Reaction Rates and Yields. *J. Am. Chem. Soc.* **2006**, *128* (2), 416−417.
(112) Zhao, J.; Yang, J.; Petek, H. Theoretical Study of the Molecular and Electronic Structure of Methanol on a TiO_2(110) Surface. *Phys. Rev. B* **2009**, *80* (23), No. 235416.
(113) Wu, W. C.; Chuang, C. C.; Lin, J. L. Bonding Geometry and Reactivity of Methoxy and Ethoxy Groups Adsorbed on Powdered TiO_2. *J. Phys. Chem. B* **2000**, *104* (36), 8719−8724.
(114) Kuznetsov, A. I.; Kameneva, O.; Alexandrov, A.; Bityurin, N.; Marteau, P.; Chhor, K.; Sanchez, C.; Kanaev, A. Light-Induced Charge Separation and Storage in Titanium Oxide Gels. *Phys. Rev. E* **2005**, *71* (2), No. 021403.
(115) Chiang, Y.-C.; Cheng, W.-Y.; Lu, S.-Y. Titania Aerogels as a Superior Mesoporous Structure for Photoanodes of Dye-Sensitized Solar Cells. *Int. J. Electrochem. Sci.* **2012**, *7*, 6910−6919.
(116) Subramanian, V.; Wolf, E. E.; Kamat, P. V. Catalysis with TiO_2/Gold Nanocomposites. Effect of Metal Particle Size on the Fermi Level Equilibration. *J. Am. Chem. Soc.* **2004**, *126* (15), 4943−4950.
(117) Enea, O.; Moser, J.; Grätzel, M. Achievement of Incident Photon to Electric Current Conversion Yields Exceeding 80% in the Spectral Sensitization of Titanium Dioxide by Coumarin. *J. Electroanal. Chem. Interfacial Elechochem.* **1989**, *259* (1−2), 59−65.
(118) Berger, T.; Sterrer, M.; Diwald, O.; Knözinger, E. Charge Trapping and Photoadsorption of O_2 on Dehydroxylated TiO_2 Nanocrystals - an Electron Paramagnetic Resonance Study. *ChemPhysChem* **2005**, *6* (10), 2104−2112.
(119) Pacchioni, G.; Ferrari, A. M.; Bagus, P. S. Cluster and Band Structure Ab Initio Calculations on the Adsorption of CO on Acid Sites of the TiO_2(110) Surface. *Surf. Sci.* **1996**, *350* (1−3), 159−175.
(120) Klimov, V. I. Optical Nonlinearities and Ultrafast Carrier Dynamics in Semiconductor Nanocrystals. *J. Phys. Chem. B* **2000**, *104* (26), 6112−6123.
(121) Ohta, N. Electric Field Effects on Photochemical Dynamics in Solid Films. *Bull. Chem. Soc. Jpn.* **2002**, *75*, 1637−1655.
(122) Hayden, B. E.; King, A.; Newton, M. A. Fourier Transform Reflection-Absorption IR Spectroscopy Study of Formate Adsorption on TiO_2(110). *J. Phys. Chem. B* **1999**, *103* (1), 203−208.
(123) Busca, G. Infrared Studies of the Reactive Adsorption of Organic Molecules over Metal Oxides and of the Mechanisms of Their Heterogeneously-Catalyzed Oxidation. *Catal. Today* **1996**, *27* (3−4), 457−496.
(124) Coronado, J. M.; Kataoka, S.; Tejedor-Tejedor, I.; Anderson, M. A. Dynamic Phenomena During the Photocatalytic Oxidation of Ethanol and Acetone over Nanocrystalline TiO_2: Simultaneous FTIR Analysis of Gas and Surface Species. *J. Catal.* **2003**, *219* (1), 219−230.
(125) Gomes, W. P.; Freund, T.; Morrison, S. R. Chemical Reactions Involving Holes at the Zinc Oxide Single Crystal Anode. *J. Electrochem. Soc.* **1968**, *115* (8), 818−823.
(126) Schwitzgebel, J.; Ekerdt, J. G.; Sunada, F.; Lindquist, S.-E.; Heller, A. Increasing the Efficiency of the Photocatalytic Oxidation of Organic Films on Aqueous Solutions by Reactively Coating the TiO_2 Photocatalyst with a Chlorinated Silicone. *J. Phys. Chem. B* **1997**, *101* (14), 2621−2624.
(127) Petek, H.; Zhao, J. Ultrafast Interfacial Proton-Coupled Electron Transfer. *Chem. Rev.* **2010**, *110* (12), 7082−7099.
(128) Dagan, G.; Tomkiewicz, M. Preparation and Characterization of TiO_2 Aerogels for Use as Photocatalysts. *J. Non-Cryst. Solids* **1994**, *175* (2−3), 294−302.
(129) Chen, L.; Zhu, J.; Liu, Y.-M.; Cao, Y.; Li, H.-X.; He, H.-Y.; Dai, W.-L.; Fan, K.-N. Photocatalytic Activity of Epoxide Sol−Gel Derived Titania Transformed into Nanocrystalline Aerogel Powders by Supercritical Drying. *J. Mol. Catal. A: Chem.* **2006**, *255* (1−2), 260−268.
(130) Hong, I. VOCs Degradation Performance of TiO_2 Aerogel Photocatalyst Prepared in SCF Drying. *J. Ind. Eng. Chem.* **2006**, *12*, 918−925.
(131) Ingale, S. V.; Wagh, P. B.; Tripathi, A. K.; Dudwadkar, A. S.; Gamre, S. S.; Rao, P. T.; Singh, I. K.; Gupta, S. Photo Catalytic Oxidation of TNT Using TiO_2-SiO_2 Nano-Composite Aerogel Catalyst Prepared Using Sol−Gel Process. *J. Sol-Gel Sci. Technol.* **2011**, *58* (3), 682−688.
(132) Zhang, Z.; Yates, J. T. Effect of Adsorbed Donor and Acceptor Molecules on Electron Stimulated Desorption: O_2/TiO_2(110). *J. Phys. Chem. Lett.* **2010**, *1* (14), 2185−2188.
(133) Rothschild, A.; Komem, Y.; Ashkenasy, N. Quantitative Evaluation of Chemisorption Processes on Semiconductors. *J. Appl. Phys.* **2002**, *92* (12), 7090−7097.
(134) Rothschild, A.; Levakov, A.; Shapira, Y.; Ashkenasy, N.; Komem, Y. Surface Photovoltage Spectroscopy Study of Reduced and Oxidized Nanocrystalline TiO_2 Films. *Surf. Sci.* **2003**, *532*−*535* (0), 456−460.
(135) Shahbazyan, T. V.; Perakis, I. E.; Bigot, J. Y. Size-Dependent Surface Plasmon Dynamics in Metal Nanoparticles. *Phys. Rev. Lett.* **1998**, *81* (15), 3120−3123.
(136) Aiboushev, A.; Gostev, F.; Shelaev, I.; Kostrov, A.; Kanaev, A.; Museur, L.; Traore, M.; Sarkisov, O.; Nadtochenko, V. Spectral Properties of the Surface Plasmon Resonance and Electron Injection from Gold Nanoparticles to TiO_2 Mesoporous Film: Femtosecond Study. *Photochem. Photobiol. Sci.* **2013**, *12* (4), 631−637.
(137) Manzoli, M.; Chiorino, A.; Boccuzzi, F. Decomposition and Combined Reforming of Methanol to Hydrogen: A FTIR and QMS Study on Cu and Au Catalysts Supported on ZnO and TiO_2. *Appl. Catal., B* **2005**, *57* (3), 201−209.
(138) Kähler, K.; Holz, M. C.; Rohe, M.; Strunk, J.; Muhler, M. Probing the Reactivity of ZnO and Au/ZnO Nanoparticles by Methanol Adsorption: A TPD and Drifts Study. *ChemPhysChem* **2010**, *11* (12), 2521−2529.

(139) Flores-Escamilla, G. A.; Fierro-Gonzalez, J. C. Participation of Linear Methoxy Species Bonded to Ti^{4+} Sites in the Methanol Carbonylation Catalyzed by TiO_2-Supported Rhodium: An Infrared Investigation. *J. Mol. Catal. A: Chem.* **2012**, *359* (0), 49−56.
(140) Rotzinger, F. P.; Kesselman-Truttmann, J. M.; Hug, S. J.; Shklover, V.; Grätzel, M. Structure and Vibrational Spectrum of Formate and Acetate Adsorbed from Aqueous Solution onto the TiO_2 Rutile (110) Surface. *J. Phys. Chem. B* **2004**, *108* (16), 5004−5017.
(141) Morikawa, Y.; Takahashi, I.; Aizawa, M.; Namai, Y.; Sasaki, T.; Iwasawa, Y. First-Principles Theoretical Study and Scanning Tunneling Microscopic Observation of Dehydration Process of Formic Acid on a TiO_2(110) Surface. *J. Phys. Chem. B* **2004**, *108* (38), 14446−14451.
(142) Uetsuka, H.; Henderson, M. A.; Sasahara, A.; Onishi, H. Formate Adsorption on the (111) Surface of Rutile TiO_2. *J. Phys. Chem. B* **2004**, *108* (36), 13706−13710.
(143) Zhang, Q.-L.; Du, L.-C.; Weng, Y.-X.; Wang, L.; Chen, H.-Y.; Li, J.-Q. Particle-Size-Dependent Distribution of Carboxylate Adsorption Sites on TiO_2 Nanoparticle Surfaces: Insights into the Surface Modification of Nanostructured TiO_2 Electrodes. *J. Phys. Chem. B* **2004**, *108* (39), 15077−15083.
(144) Berger, T.; Delgado, J. M.; Lana-Villarreal, T.; Rodes, A.; Gomez, R. Formate Adsorption onto Thin Films of Rutile TiO_2 Nanorods and Nanowires. *Langmuir* **2008**, *24* (24), 14035−14041.
(145) Tabakova, T.; Boccuzzi, F.; Manzoli, M.; Andreeva, D. FTIR Study of Low-Temperature Water-Gas Shift Reaction on Gold/Ceria Catalyst. *Appl. Catal., A* **2003**, *252* (2), 385−397.
(146) DeSario, P. A.; Pietron, J. J.; DeVantier, D. D.; Brintlinger, T. H.; Stroud, R. M.; Rolison, D. R. Plasmonic Enhancement of Visible-Light Water Splitting with Au−TiO_2 Composite Aerogels. *Nanoscale* 2013, *5*, in press; DOI: 10.1039/C3NR01429K.